NAVAL POSTGRADUATE SCHOOL
Monterey, California

THESIS

PARAMETRIC X-RADIATION FROM A BERYLLIUM CRYSTAL

by

David J. Hauth

September 1999

Thesis Advisor: Xavier K. Maruyama
Second Reader: Melvin A. Piestrup

Approved for public release; distribution is unlimited.

REPORT DOCUMENTATION PAGE

Form Approved OMB No. 0704-0188

1. AGENCY USE ONLY *(Leave blank)*	2. REPORT DATE	3. REPORT TYPE AND DATES COVERED
	September 1999	Master's Thesis

4. TITLE AND SUBTITLE
PARAMETRIC X-RADIATION FROM A BERYLLIUM CRYSTAL

5. FUNDING NUMBERS

6. AUTHOR
Hauth, David J.

7. PERFORMING ORGANIZATION NAME(S) AND ADDRESS(ES)
Naval Postgraduate School
Monterey, CA 93943-5000

8. PERFORMING ORGANIZATION REPORT NUMBER

9. SPONSORING / MONITORING AGENCY NAME(S) AND ADDRESS(ES)

10. SPONSORING / MONITORING AGENCY REPORT NUMBER

11. SUPPLEMENTARY NOTES
The views expressed in this thesis are those of the author and do not reflect the official policy or position of the Department of Defense or the U.S. Government.

12a. DISTRIBUTION / AVAILABILITY STATEMENT
Approved for public release; distribution unlimited.

12b. DISTRIBUTION CODE

13. ABSTRACT *(maximum 200 words)*

A source of monochromatic x-rays in the 16 keV to 24 keV range will provide improved contrast and overall image quality in mammography while also reducing overall patient dose [Ref. 6,7]. Based on theoretical work by Freudenberg [Ref. 6,9], beryllium (Be) was identified as a candidate to be a more efficient source of PXR based x-radiation in this energy range. This thesis describes the use of the NPS 100 MeV linear accelerator (LINAC) to conduct the first parametric x-radiation (PXR) experiments using a beryllium (Be) crystal. Energy spectra were collected from the beryllium crystal that differed from theoretical prediction. This thesis explores explanations of the spectra and provides a foundation of understanding of beryllium crystals for future experiments.

14. SUBJECT TERMS
Parametric x-radiation, Beryllium, Close-packed Hexagonal Crystal, Mammography

15. NUMBER OF PAGES
67

16. PRICE CODE

17. SECURITY CLASSIFICATION OF REPORT	18. SECURITY CLASSIFICATION OF THIS PAGE	19. SECURITY CLASSIFI- CATION OF ABSTRACT	20. LIMITATION OF ABSTRACT
Unclassified	Unclassified	Unclassified	UL

NSN 7540-01-280-5500

Standard Form 298 (Rev. 2-89)
Prescribed by ANSI Std. 239-

THIS PAGE INTENTIONALLY LEFT BLANK

Approved for public release; distribution is unlimited

PARAMETRIC X-RADIATION FROM A BERYLLIUM CRYSTAL

David J. Hauth
Lieutenant, United States Navy
B.S., United States Naval Academy, 1991

Submitted in partial fulfillment of the
requirements for the degree of

MASTER OF SCIENCE IN PHYSICS

from the

NAVAL POSTGRADUATE SCHOOL
September 1999

Author: _____
David J. Hauth

Approved by: _____
Xavier K. Maruyama, Thesis Advisor

_____
Melvin A. Piestrup, Second Reader

_____
William B. Maier, II, Chairman
Department of Physics

THIS PAGE INTENTIONALLY LEFT BLANK

ABSTRACT

A source of monochromatic x-rays in the 16 keV to 24 keV range will provide improved contrast and overall image quality in mammography while also reducing overall patient dose [Ref. 6,7]. Based on theoretical work by Freudenberg [Ref. 6,9], beryllium (Be) was identified as a candidate to be a more efficient source of PXR based x-radiation in this energy range. This thesis describes the use of the NPS 100 MeV linear accelerator (LINAC) to conduct the first parametric x-radiation (PXR) experiments using a beryllium (Be) crystal. Energy spectra were collected from the beryllium crystal that differed from theoretical prediction. This thesis explores explanations of the spectra and provides a foundation of understanding of beryllium crystals for future experiments.

THIS PAGE INTENTIONALLY LEFT BLANK

TABLE OF CONTENTS

THIS PAGE INTENTIONALLY LEFT BLANK

ACKNOWLEDGEMENTS

I would like to thank everyone who helped in the completion of this thesis. Without Don Snyder's infinite patience and experience with the LINAC this thesis would have never been completed. Mel Piestrup, Charles Gray, and Héctor Raúl Beguiristain of Adelphi Technology provided knowledge and materials in support of this thesis. Lastly, I would like to thank X. K. Maruyama, whose patience was never tried despite my continually setting deadlines and breaking them.

I. INTRODUCTION

X-ray tube technologies are the predominate means of conducting mammographs for breast cancer screening. One of the difficulties encountered in mammography is that at typical x-ray tube energies (nominally about 40 keV) there is little difference in the absorption properties of cancerous and noncancerous cells. As a result, small cellular anomalies (on the order of 2-3 mm) can only be detected through indirect means such as microcalcification or distortions seen in the x-ray image of the surrounding tissue [Ref. 5]. It has been shown that at energies between 16 keV and 22 keV, contrast is improved and greater detail is revealed [Ref. 7]. However, lower energies require longer exposure times. With x-ray tube technologies, the band of x-radiation produced is very broad, and the patient is exposed to radiation that does not contribute to the image. The result is an increased radiation dose to the patient. A monochromatic source, then, is desirable because the patient is exposed only to the radiation required to generate the x-ray image. In addition, if a tunable source of monochromatic x-rays could be developed, use might be made of the photoelectric effect and the absorption edges of physiological atoms to allow chemical analysis of anomalies visible in the x-ray image. Subtraction imaging would also be possible [Ref. 5]. Mammography, then, requires a hard x-ray source with the following properties: monochromatic, tunable with energy from 16 keV to 24 keV, relatively inexpensive, low patient dose.

Currently, synchrotron facilities using monochromators are the only source of monochromatic hard x-rays with sufficient spectral power density to meet the above requirements. However, to achieve such energies, GeV storage rings are required at cost of over $60 million [Ref. 5]. Very few medical facilities can afford such a capital expenditure.

It has been shown that parametric x-radiation (PXR) is a compact, tunable source of monochromatic hard x-rays with energies of hundreds of eV to tens of keV [Ref. 6]. Additionally, PXR is independent of incident electron energy and allows use of small LINACs with energies on the order of 20-50 MeV to achieve the desirable x-ray energies. PXR has the additional benefit that it is not collinear with the electron beam. It is most intense at an angle measured relative to the velocity vector of the incident electron and therefore removes the patient from the bremsstrahlung background.

PXR results from the interaction of a relativistic electron ($E >> mc^2$) with the atomic planes of a crystal. A relativistic charged particle's electromagnetic field can be represented as a superposition of virtual photons. The interaction of the electron beam with the crystal can then be thought of as the interaction of a beam of photons with the crystal [Ref. 1]. Those virtual photons that satisfy the Bragg condition ($(\kappa+\tau)^2 \approx \kappa^2$) are diffracted by the crystal and manifest themselves as x-radiation about the Bragg angle measured relative to the incident electron's velocity vector.

The theory of PXR was first developed by Ter-Mikaelian in 1971. The theory was confirmed experimentally in 1985 by Baryshevsky [Ref. 3]. The first PXR experiments to be conducted outside the former Soviet Union were done at Naval Postgraduate School in the early 1990's. Those experiments focused on determining whether PXR was a viable candidate as a compact tunable x-ray source and proved to be very successful.

Feranchuck theorized that the density of atoms in the crystal was directly related to the crystal's ability to produce PXR radiation. Feranchuck determined that crystals with diamond based unit cell structure would be the most favorable, focusing specifically on C, Ge, and Si. Previous experiments at NPS and other facilities have focused on C and Si crystals.

Freudenberger has developed an alternate theory to predict a crystal's ability to act as a PXR radiator. This theory develops an expression for PXR intensity, $P_{crystal}$, which predicts that Be should be the most efficient PXR radiator in the 20 keV region [Ref. 9].

This thesis conducted the first PXR experiment using a Be crystal. The last PXR experiment performed at NPS was three years prior. As a result, many of the experimental procedures that evolved from past experience had to be researched and recreated. Additionally, the NPS LINAC had to be brought back to operational status after several vacuum leaks were discovered and repaired in the beam pipe.

The resulting data from the experiment matched theoretical energy calculations done prior to the experiment, but also contained some unexpected results. This thesis attempts to reconcile the results with theory. Also, initial indications of photon yield do not support Freudenberger's assertion that Beryllium is an ideal source of hard x-rays in the 20 keV region. Collection of further data to aid in the assessment of the PXR characteristics of beryllium was curtailed when flooding of the accelerator facility severely damaged the LINAC.

THIS PAGE INTENTIONALLY LEFT BLANK

II. BERYLLIUM TARGET

The beryllium crystal has a hexagonal close-packed (HCP) unit cell structure. The HCP structure is simply a hexagonal base of six atoms and one additional atom in the center as shown in Figure 1(a). On top of that base are stacked three more atoms and then seven more forming another hexagon. This is depicted in Figure 1(b) and Figure 1(c). The crystal structure mimics an optimal spherical packing problem, much the same as stacking oranges for a grocery display and demonstrates the ABA close-packing pattern.

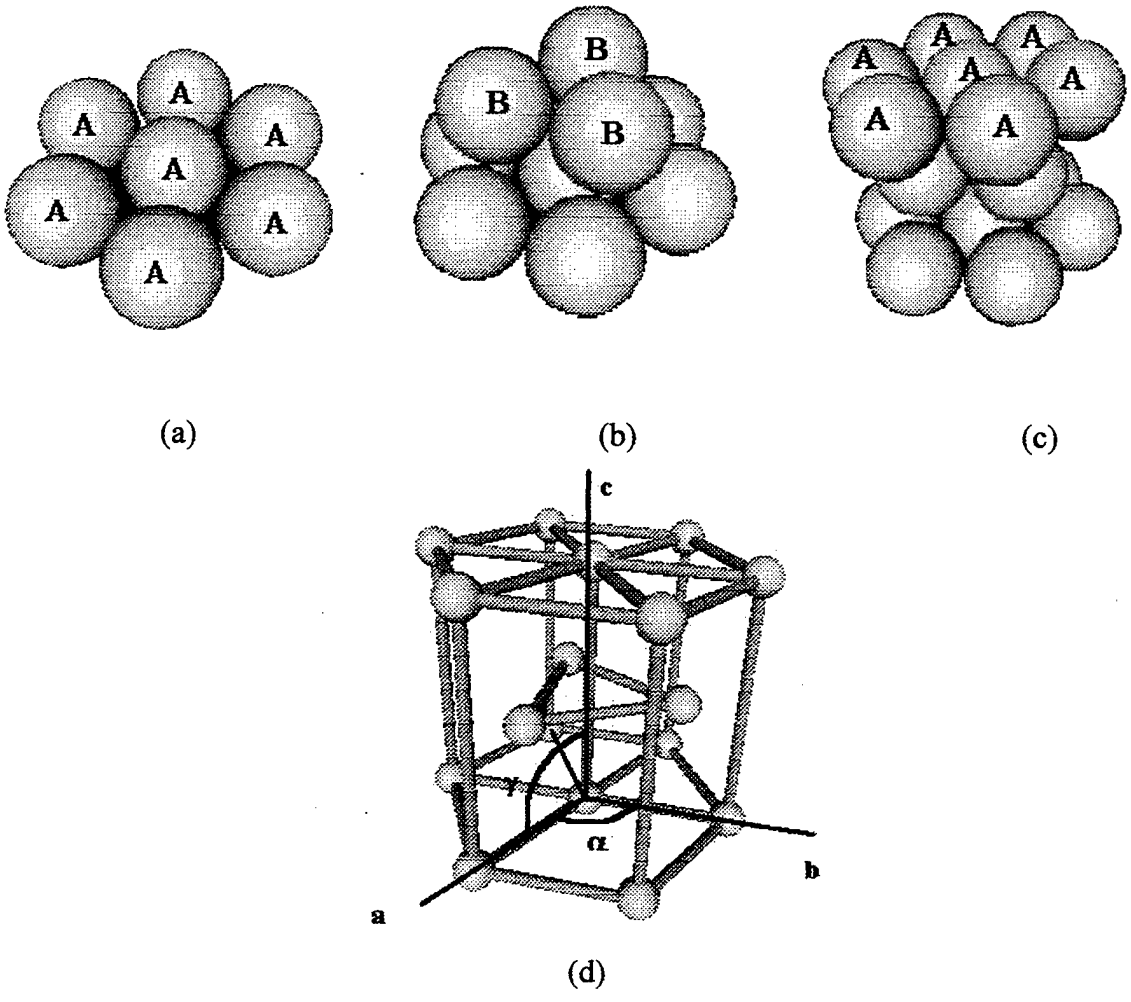

Figure 1. The Relationship of Atoms for HCP Crystals. (a-c) The ABA close-packing pattern is depicted (d) Definition of HCP crystal cell parameters. The angle β is not shown but is equal and symmetric to α.

Crystal cell parameters for Beryllium are as follows: **a** = **b** = 2.28 Å, **c** = 3.58 Å, $\alpha = \beta = 120°$, $\gamma = 90°$ as shown in Figure 1(d). The dimensions of the target crystal were 4.5mm x 5.5mm x 0.5mm. The 4.5mm x 5.5mm face corresponded with the (1-100) plane, the 5.5 mm x 0.5mm edge corresponded with the (0001) plane, and the 4.5 mm x 0.5 mm edge the (11-20) plane.

Since the energy of the emitted PXR radiation is dependent on the Bragg relation ($\lambda = 2d \sin\theta$), for a fixed angle, the interplanar spacing of the crystal dictates the energies available from that crystal. When the 4.5 mm x 5.5 mm face of the crystal is parallel to the beam, turning it 22.5° counterclockwise satisfies the Bragg relation for the (1-100) plane, while turning it 112.5°counterclockwise satisfies the Bragg relation for the (0001) plane. This is shown in Figure 2(a) and Figure 2(b).

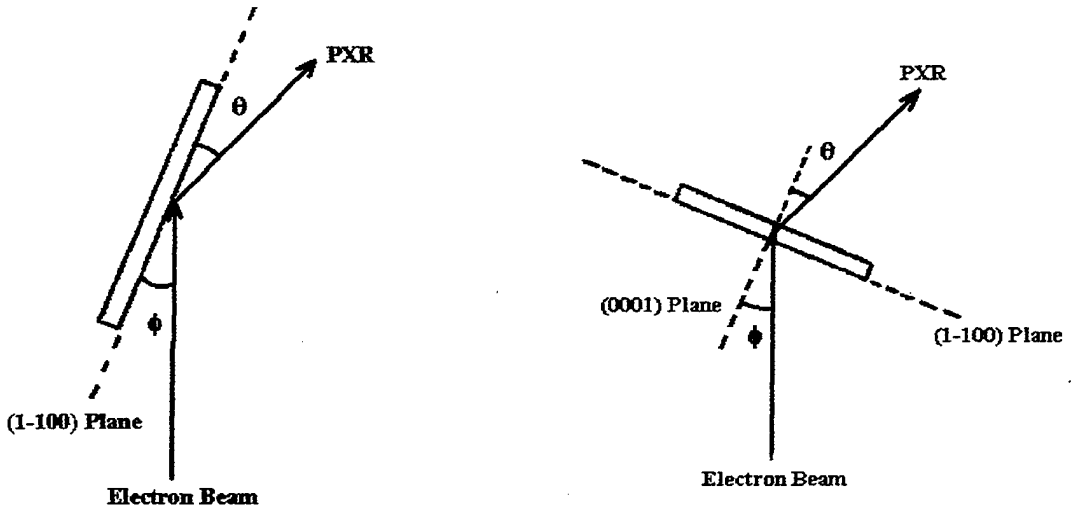

(a) (b)

Figure 2. PXR Geometries with Be Crystal (a) The geometry of the Be crystal, electron beam and PXR for (1-100) plane. $\phi = \theta = 22.5°$(b) The geometry of the Be crystal, electron beam and PXR for (0001) plane. $\phi = \theta = 22.5°$

With the (1-100) plane turned to 22.5° relative to the incident electron beam, the crystal has three separate planes that simultaneously satisfy the Bragg relation. The first plane is formed by the atoms labeled **f** and **a**, the second plane by atoms **o** and **m**, and the third plane by **e**, **g**, and **b**. The (1-100) plane of the crystal is depicted in Figure 3(a). Figure 3(b) shows that the three planes have spacings of x = 0.66 Å, y = 1.32 Å and x + y = 1.98 Å.

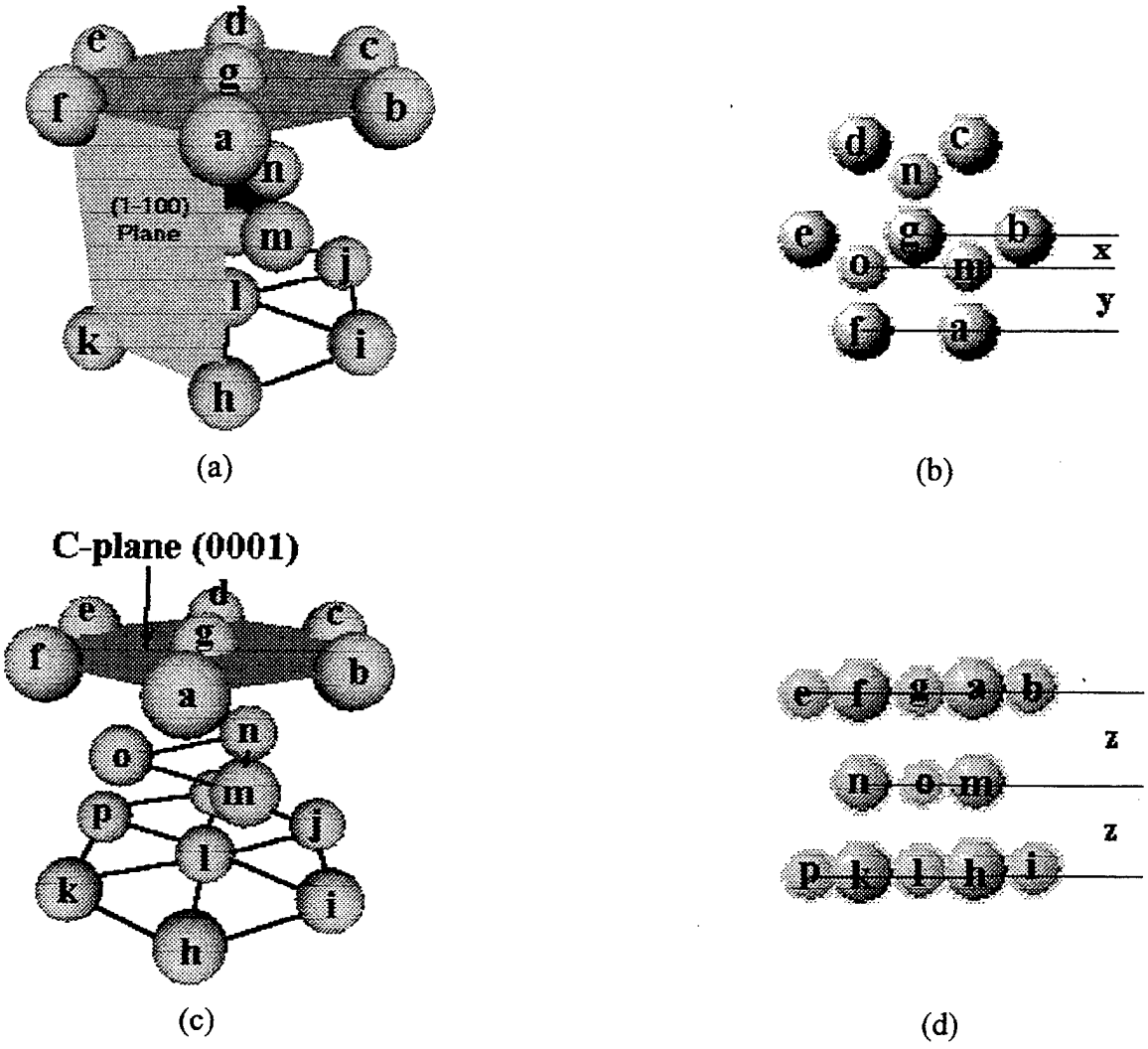

Figure 3. Planes and Planar Spacing of Be Crystal (a) The (1-100) plane is depicted. (b) The spacing of the planes parallel to (1-100). x = .66 Å, y = 1.32 Å, and x + y = 1.98 Å. (c) The (0001) plane is depicted. (d) The spacing of the (0001) and (0002) planes is shown. z = 1.79 Å.

Figure 3(c) and Figure 3(d) show the relationship and spacing of the "C" plane. The three center atoms, **m**, **n**, and **o**, from Figure 3(c) divide the crystal cell in half, resulting in an interplanar spacing of 1.79 Å and 3.58 Å. The Miller indices of the center plane are (0002). By combining the constants, the Bragg relationship can be reduced to the following formula for energy at the given Bragg angle (in this case 22.5 degrees):

$$E = \frac{16.20\ \text{keV} \cdot}{d}\ \text{Å}. \qquad (1)$$

where d is the interplanar spacing in Å. Applying equation (1) to the geometry illustrated in Figure 3(a) and Figure 3(b) gives energies of 8.18 keV, 12.2 keV, and 24.5 keV for three first order planes with interplanar spacing of 1.98 Å, 1.32 Å, and 0.66 Å respectively. Equation (1) gives energies of 4.54 keV and 9.05 keV for the planes in Figure 3(c) and Figure 3(d) with interplanar spacing of 3.58 Å and 1.79 Å respectively.

III. EXPERIMENTAL DESCRIPTION

The experiment was conducted in December 1998 using the NPS Linear Accelerator (LINAC). A beryllium crystal was placed in the target chamber of the LINAC with its (0001) plane positioned in the Bragg geometry relative to the velocity vector of the incident electrons (Figure 2(b)). The crystal was held in a target ladder which could be remotely rotated about its vertical and horizontal axis by a computer controlled goniometer whose angular resolution was about .01°. In addition, the ladder can be raised or lowered to position different targets in the beam line. Copper (Cu), Tin (Sn) and phosphorescent foils were placed in "rungs" below the crystal to act as calibration sources and to aid in experimental alignment. A Canberra solid state Si(Li) detector was positioned at the 45° instrument port relative to the beam to measure the resulting radiation. The LINAC and basic experimental set-up are shown in Figure 4.

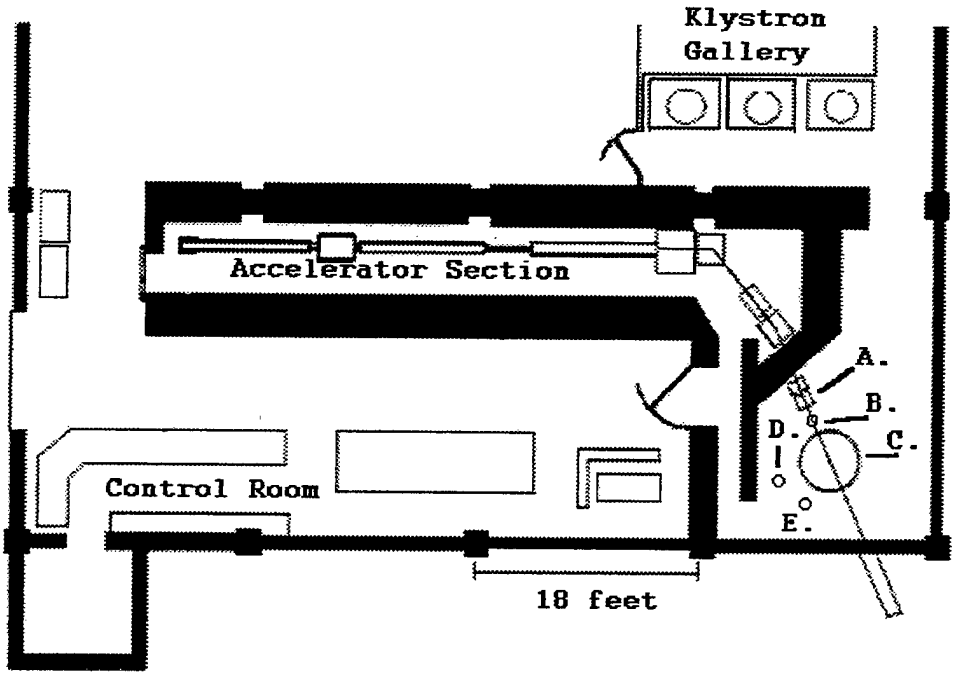

Figure 4. General Layout of the LINAC and Experimental Apparatus. A - Quadrupole magnets, B - end station steering magnets, C - target chamber, D - alignment laser, E - detector.

A. EXPERIMENTAL ALIGNMENT

Consistent and accurate experimental alignment are critical in PXR experiments. Relative alignment between the electron beam, the target and the detector must be accurately established to ensure that the proper conditions are met to generate PXR and the detector is optimally placed relative to the target to collect the radiation.

The geometric center of the target chamber was chosen to be the reference point for the mutual alignment of the beam, the target and the detector. The target chamber is a machined circle with instrumentation/viewing ports and beam entry/exit ports established at precise angles around that circle. To establish proper alignment, viewing ports on opposite sides of the chamber were blocked off with alignment masks. These masks had pinholes drilled in their centers. A straight line extending between these holes passes through the geometric center of the chamber. A laser was made to pass through both holes and strike an additional reference mark external to the chamber. Once alignment was established, the laser was fixed in position and acted as the reference standard. A small mirror was fixed to the ladder such that its surface was coplanar with that of the target crystal. To establish the zero or "home" position the laser was rotated and tilted until retroreflection was achieved. The mirror was then rotated 45° and the Si(Li) detector aligned so that the reflected laser beam was centered on its detection window. The ladder was now raised so that the phosphorescent foil was in the beam line. The foil had a pinhole in its center that was aligned with the center of the target chamber. Tilt, rotation and ladder height were adjusted so that the laser passed through the pinhole. The screen was then rotated so that its face was perpendicular to the beam line. Beam was established in the LINAC and was clearly visible on the phosphorescent foil. The beam alignment and end station steering magnetic were used to establish a small beam and steer it through the pinhole. For PXR measurements, the target was lowered until the reference laser was centered on its face and then

rotated to the proper angle for the experiments. In this manner it was assured that the electron beam passed through the center of the chamber, the target was positioned in the center of the chamber, the angle between the crystal and the beam was known and the angle between the crystal and the detector was also known.

B. SPECTROSCOPY/DATA COLLECTION

Spectroscopic setup and data collection procedures mirrored those established by previous PXR experiments at NPS. These procedures are based on the fact that the NPS LINAC operates at 2856 MHz with a pulse repetition rate of 60 Hz. The beam macro structure length is approximately 1 μs. This dictates a count rate of 60 MHz when a single photon is detected during each LINAC pulse.

In contrast, a Si(Li) detector's ability to distinguish between to the arrival of two photons separated in time is determined by its response time and the shaping function employed. A Si(Li) detector registers an incident photon as a voltage difference across a pn type junction. After the initial peak, the voltage decays exponentially. This results in the event being stretched in time. If the intensity of the incident photons is sufficiently high, the detector can not recover fast enough resulting in pulse pile-up. Most preamplifiers employ some sort of shaping function to combat this. The shaping function reshapes the decaying exponential as a square pulse that contains the voltage peak, but eliminates the extended tail.

For this experiment the shaped pulse from the Canberra detector was 12 μs in length. Because the pulse length of the detector is longer than that dictated by the LINAC duty cycle, pulse pile-up is a large problem when doing PXR experiments. When two photons arrive at the detector separated in time by less than the pulse shaping time of the detector, the two photons are registered as one photon with twice the energy. PXR is characterized by peaks that are periodic

in energy. Pulse pile-up, then, results in an incorrect distribution of PXR intensity with respect to energy. Previous experiments at NPS determined that limiting the LINAC to five to ten pulses to every detector count reduced pulse pile-up to levels compatible with the overall experimental accuracy. To accommodate this, the LINAC had to be operated under using "dark current." Dark current operations refer to LINAC operation with the gun grid voltage turned off. Stray electrons are picked up by the LINAC and accelerated resulting in average currents on the order of $1x10^{-14}$ Amperes.

An additional source of experimental difficulty is due to the noise generated by the LINAC klystrons and accelerating structure. Previous PXR experiments developed a gating system to reduce this noise. This system is shown in Figure 5.

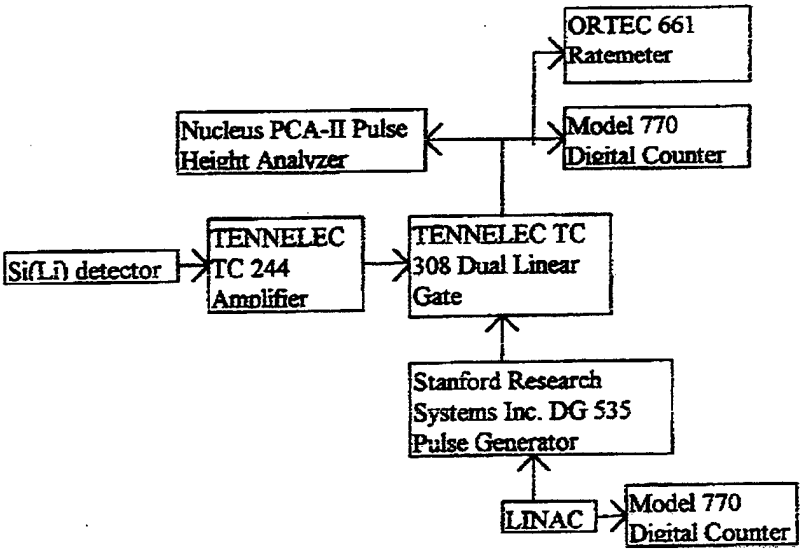

Figure 5. Spectroscopic Signal Flow

A linear gate is employed that only allows signal from the detector to be available to the pulse height analyzer (PHA) during a machine pulse. The delays were adjusted so that the PHA

was gated to be on slightly before the LINAC pulse arrived at the target. An inherent problem with this method is that the klystron noise cycle is sinusoidal in nature and PHA on-time gate consistently coincides with the negative part of portion of this cycle. Because the Si(Li) detector is registering a voltage differential, this negative background provides a bias to those voltages lowering the apparent energy of the incident photon. To combat this, energy calibration is done in the radiation environment using x-ray fluorescence from Cu and Sn foils.

C. ENERGY CALIBRATION

Before each PXR experiment an initial calibration was conducted using ^{55}Fe and ^{137}Cs radioactive sources with the LINAC off. An example is shown in Figure 6. This afforded the opportunity to check all spectroscopic systems before going through the involved process of turning on the LINAC. In addition, amplifier gain and PHA low level discriminator adjustments could be optimized for predicted PXR energy levels prior to startup.

Energy calibration is completed by the PHA software after some input by the user. After collecting a spectrum, the PHA software was used to do a peak search. The software fits a Gaussian to the peaks and determines the centroid. After the user enters energies for the peaks, the software does a linear fit by channel based on the known energies. After completing the initial calibration, system checkout and alignment procedure dark current was established in the LINAC and the Cu and Sn foils were raised into the beam line. Dark current electrons incident on the foils knock electrons out of the Cu and Sn atoms. As electrons from outer orbitals jump down to fill the holes they give up a discrete quanta of energy in the form of a x-ray.

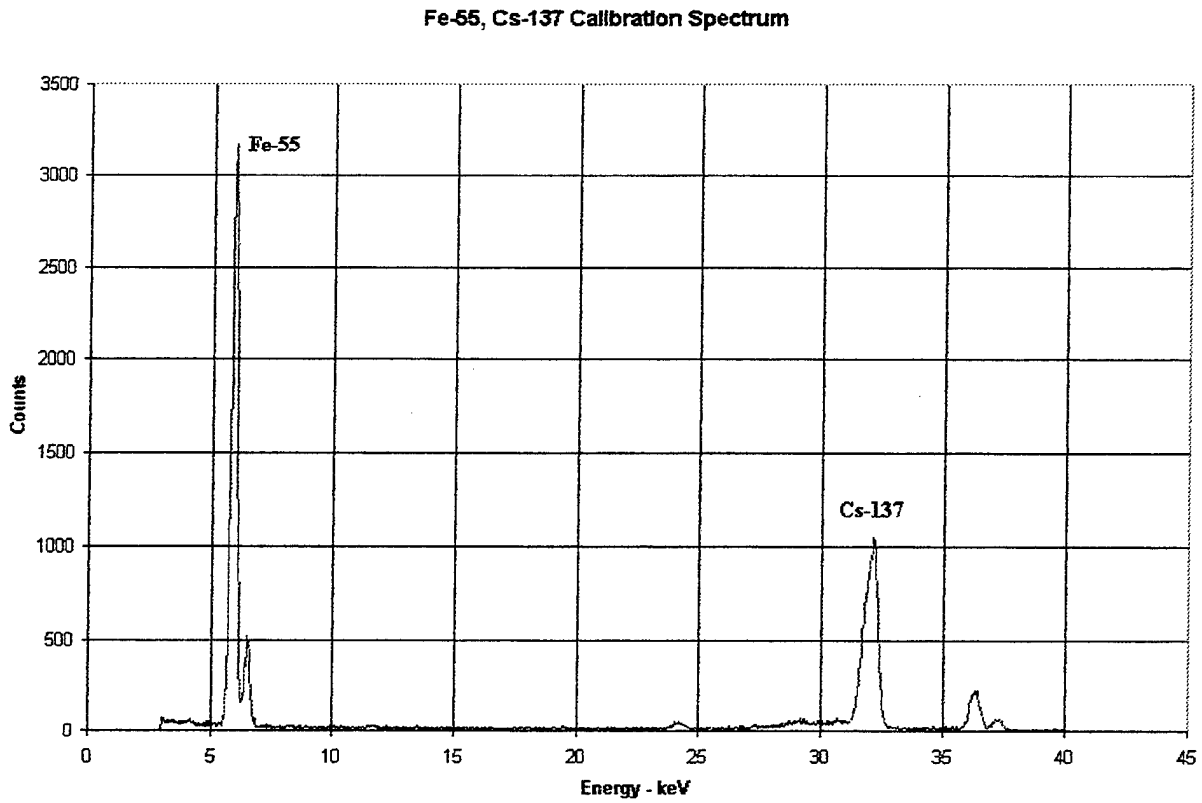

Figure 6. A Static Calibration Using ^{55}Fe and ^{137}Cs. ^{55}Fe decays by electron capture. The daughter nucleus for the decay is ^{55}Mn. The 5.9 keV and 6.49 keV peak correspond to the K_α and K_β lines of Mn. ^{137}Cs decays in the same manner with Ba as the daughter nucleus. The 32.1 keV and 36.6 keV peaks correspond to the K_α and K_β lines of Ba.

Over time this results in a peak centered on the K_α emission energy. These peaks were used to recalibrate the PHA software for the radiation environment of the LINAC and minimized the bias incurred from klystron and accelerator structure noise. An example of a characteristic x-ray spectrum is shown in Figure 7. The Cu and Y (Yttrium) K_α and K_β lines at 8.05, 8.9, 14.9, 16.7 keV are easily discernable. The Sn K_α is visible at 25.3 keV.

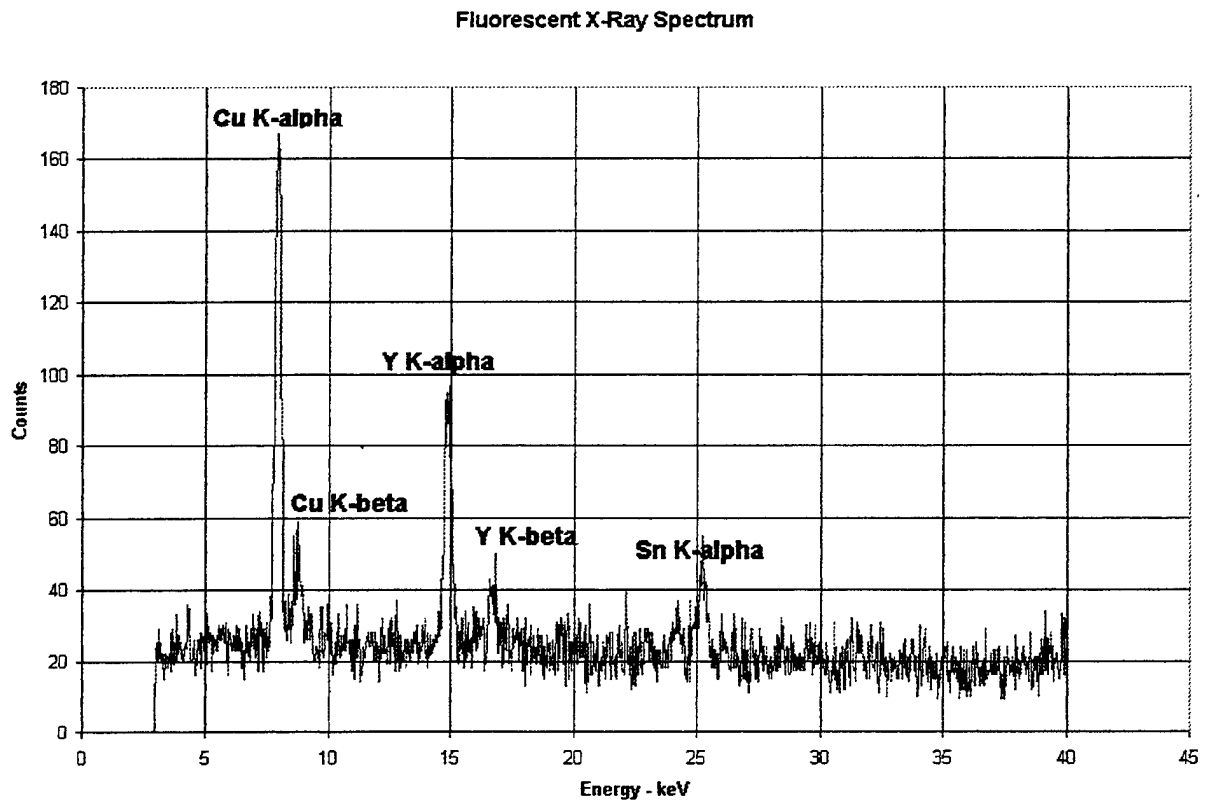

Figure 7. Characteristic X-ray Calibration Spectrum. The Cu and Y (Yttrium) K_α and K_β lines at 8.05, 8.9, 14.9, 16.7 keV are easily discernable. The Sn K_α is visible at 25.3 keV.

THIS PAGE INTENTIONALLY LEFT BLANK

IV. ANALYSIS OF BERYLLIUM PXR SPECTRUM

A total of 22 energy spectra were collected from the Beryllium crystal. The crystal was rotated to the Bragg angle corresponding to the (0001) plane. Since there is an angular dependence carried in the Bragg relation, PXR is most intense at angles close to the Bragg angle. Many of the spectra, therefore, focused on determining the optimal angle for the experimental configuration since exact alignment of the crystal planes with the target ladder can not be assured. Theoretical energy value for a first order reflection was expected to be 9.05 keV. All spectra are shown in the appendix.

The final PXR experiment was conducted on 15 Dec 98. The collection time was extended to 3 hours and 20 minutes to obtain better counting statistics and improve the signal to noise ratio of the spectrum. Of primary interest was obtaining a spectrum that included the higher order "reflections" that typify PXR.

Figure 8 shows such a spectrum obtained from a graphite crystal. This spectrum was taken in preparation for experiments with the beryllium crystal to ensue that experimental conditions produced data equivalent to previous PXR experiments at NPS. The higher order "reflections" are clearly evident out to seventh order.

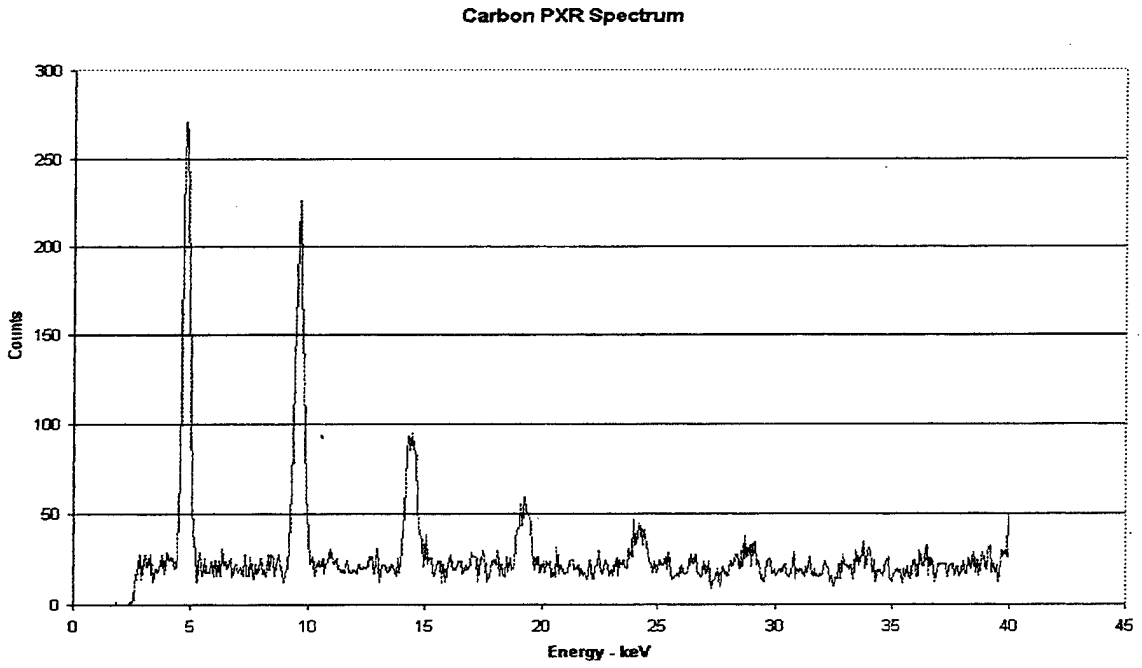

Figure 8. Carbon PXR Spectrum. Energy peaks out to N =7 are evident.

The raw spectrum obtained during the final experiment is shown in Figure 9. The spectrum was corrected for detector efficiency (Figure 10) and the average background removed. The resulting spectrum is show in Figure 12. No higher order "reflections" are evident. Instead, two distinct peaks are seen at 9.83 keV and 24.9 keV. Post experiment calibration indicated that these energies are high by approximately 750 eV. The distinct energy peaks, then, are at 9.1 keV and 24.15 keV. Additional structure can be seen at approximately 18 keV and 27 keV. The broad energy peak at 18 keV is not characteriestic of PXR and probably due to pulse pile-up. The weak energy peak at 27 keV may be attributed to the third order "reflection" of the 9.1 keV peak. Neither peak is considered here. The pertintent information is summarized in Table 1.

Raw Peak Energy - keV	Corrected (-750 ev)	Expected/Unexpected
9.85	9.1	Expected
24.9	24.15	Unexpected

Table 1.

As stated earlier, the expected energy from the (0002) plane was 9.05 keV. If the 9.1 keV peak is attributed to PXR, the absence of a distinct second order reflection and the presence of the 8.18 keV and 24.15 keV peaks is unexpected. The 8.18 keV is an artifact of the removing the background noise. When the spectrum is averaged The narrow line width of both peaks implies that they result from either discrete processes or diffraction phenomenon.

The following explanations are considered: A. The peaks are LINAC or other instrument induced noise. B. The peaks are fluorescent x-ray edges. C. The peaks are the result of residual radioactivity in the LINAC endstation. D. The peaks are PXR from the target ladder. E. The peaks are the results of other coherent x-ray processes. F. The assumed geometry is incorrect and the peaks are PXR from the (1-100) geometry shown in Figure 3(a) and Figure 3(b). In this case, an explanation must be provided for the 9.1 keV peak. G. The peaks are the result of growth and deformation faults in the HCP structure.

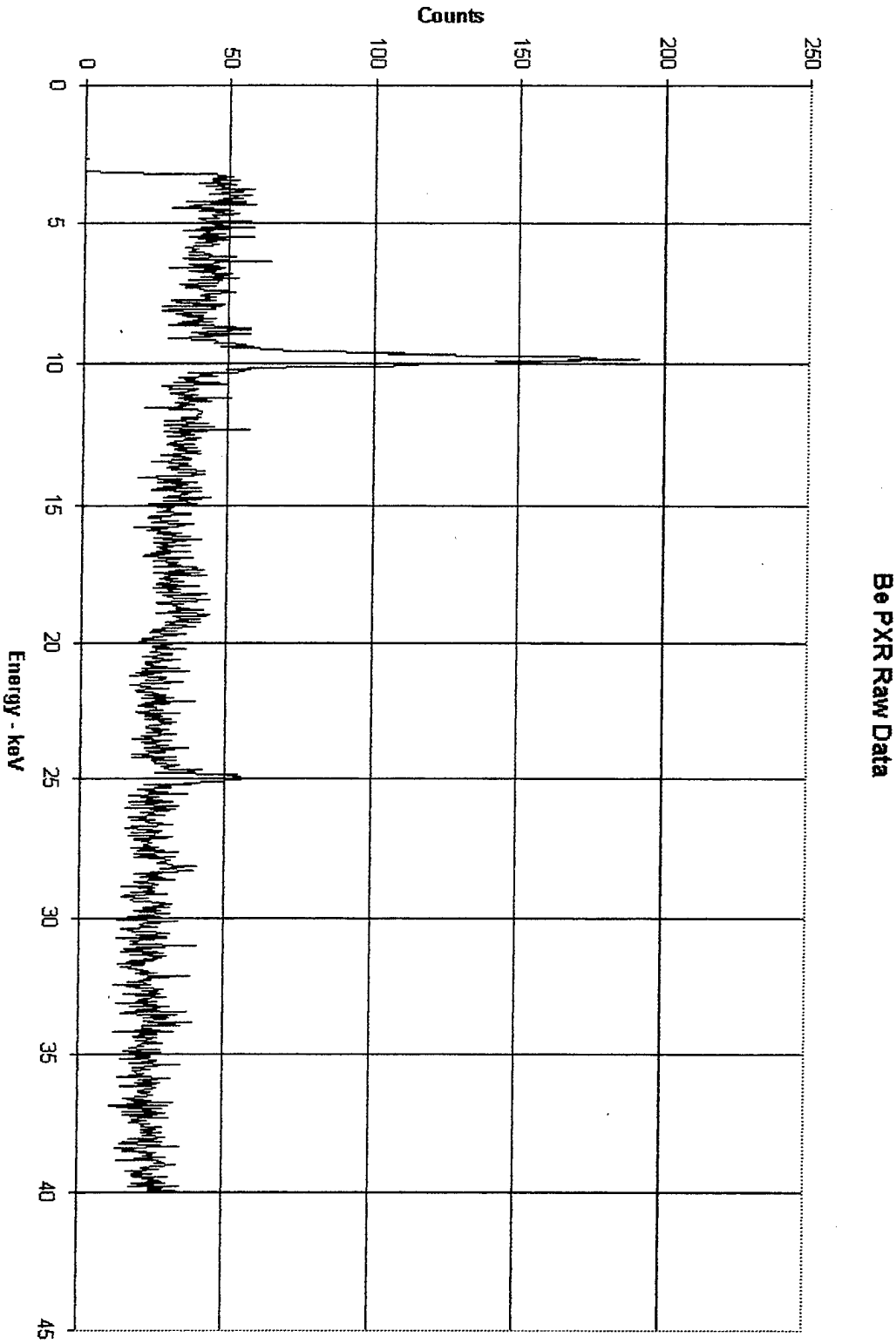

Figure 9. Raw Be PXR Spectrum. Collection time was 3 hours 20 minutes. Energy peaks are clearly evident at 9.85 keV and 24.9 keV.

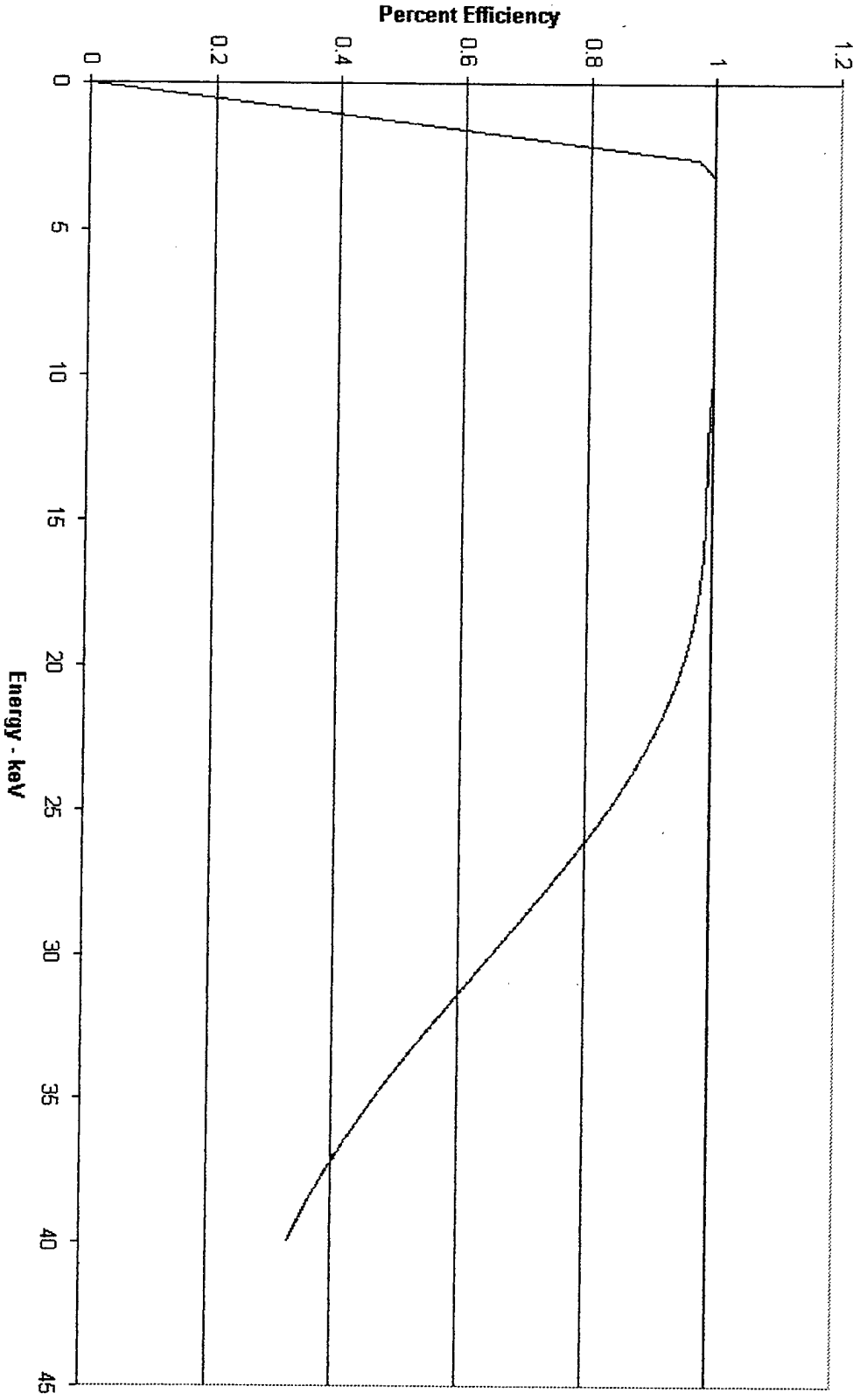

Figure 10. Si(Li) Detector Efficiency

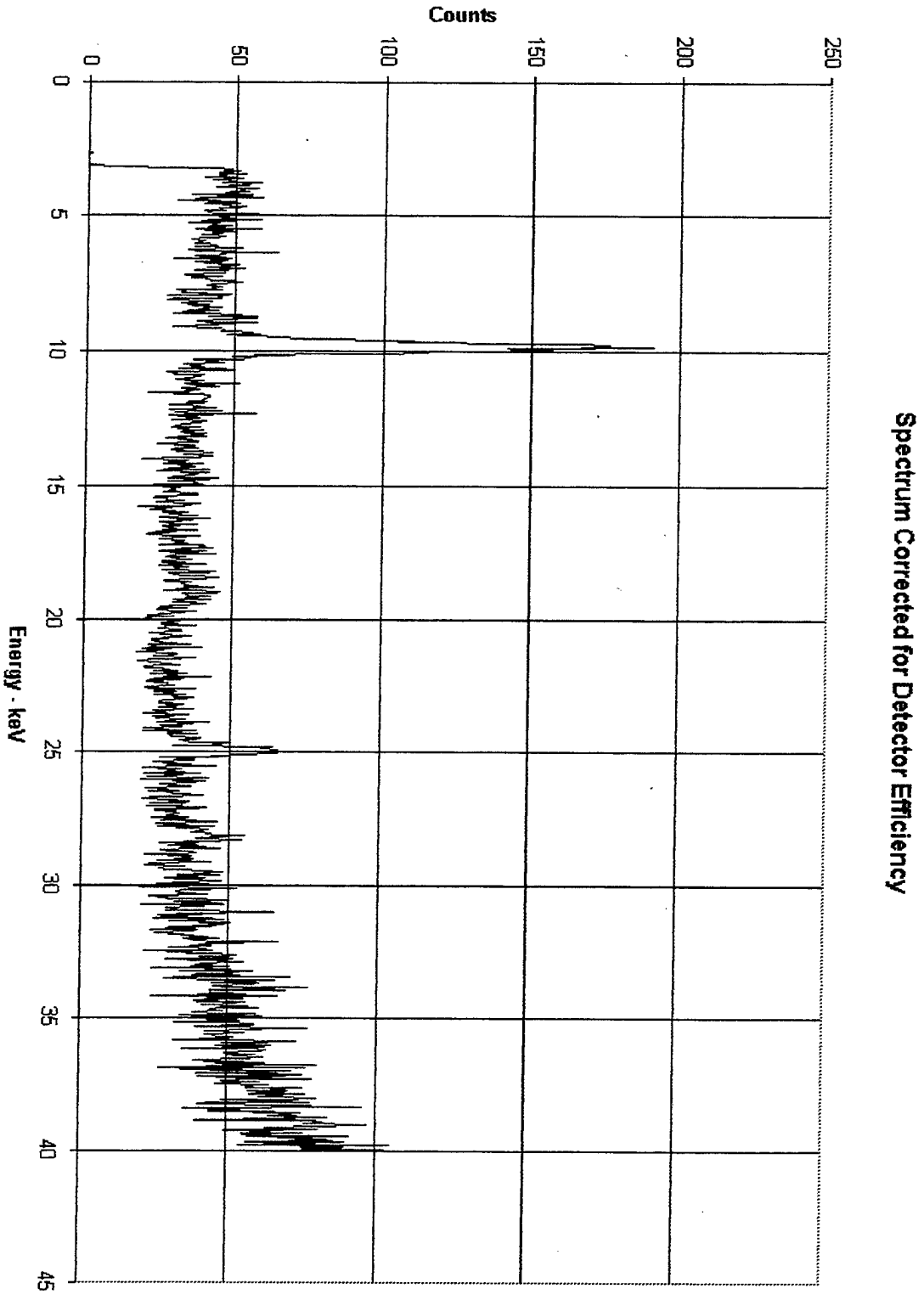

Figure 11. Raw Be PXR Spectrum. Spectrum has been corrected for detector efficiency. Limitations in the detector's efficiency make the spectrum too noisy to be of use above above 30 keV.

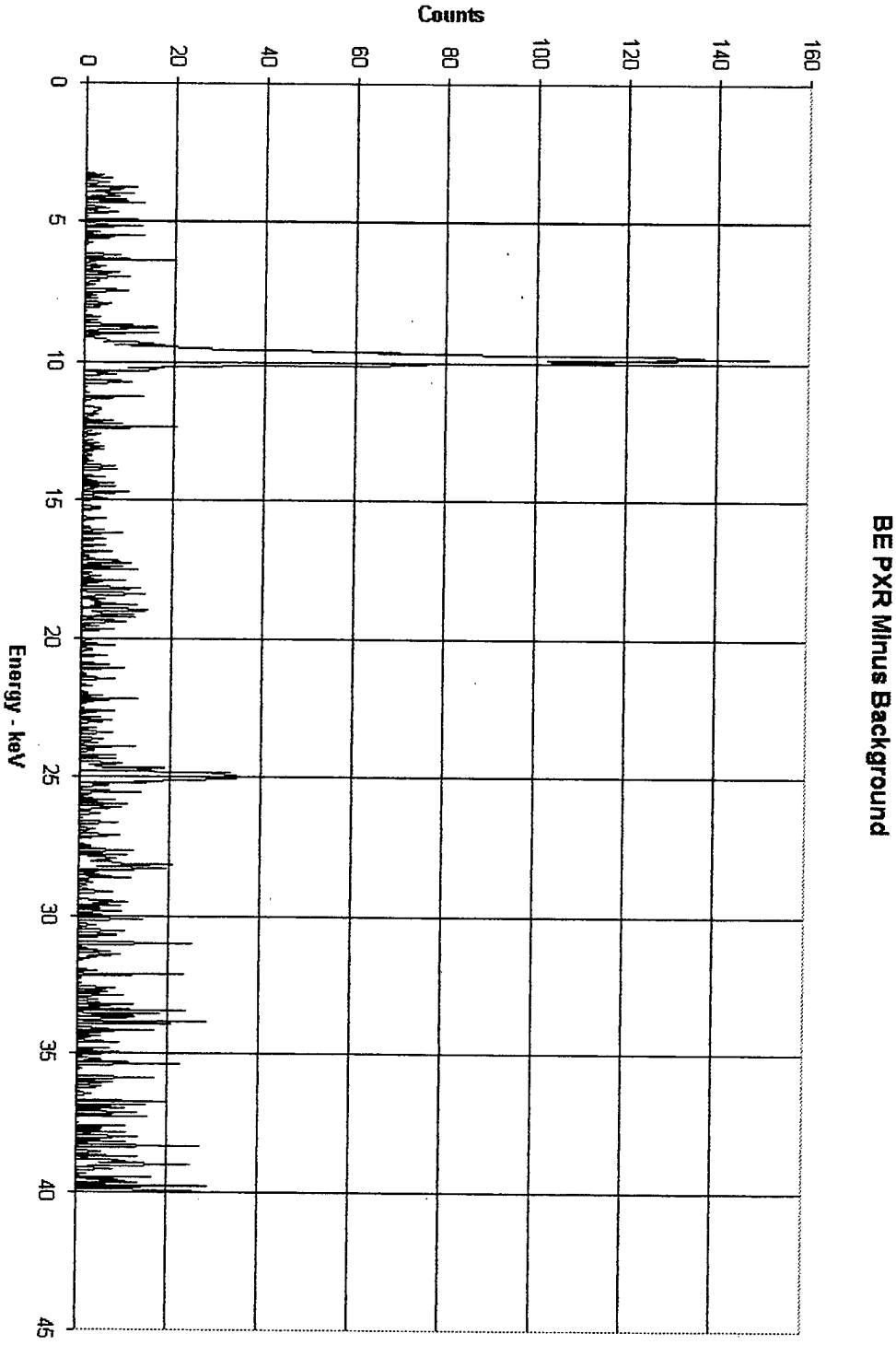

Figure 12. The Efficiency Corrected Be PXR Spectrum with Background Removed. Peaks at 9.85 keV, and 24.98 keV are readily apparent. The energy calibration is known to be 750 eV high. The corrected peaks are at 8.18 keV, 9.1 keV, and 24.15 keV.

A. LINAC INDUCED NOISE

It is unlikely that the 24.15 keV peak is due to LINAC or other instrument noise. If this were the case, these peaks would be evident in other spectra with long collection times. These peaks would also have be evident in previous experiments conducted with the LINAC. Such has not been the case. Figure 13 is a spectrum of the background noise in the end station with the klystrons running. The noise is distributed over a wide energy range and contains no discrete energy signatures. Therefore LINAC or other instrument noise does not explain the spectrum.

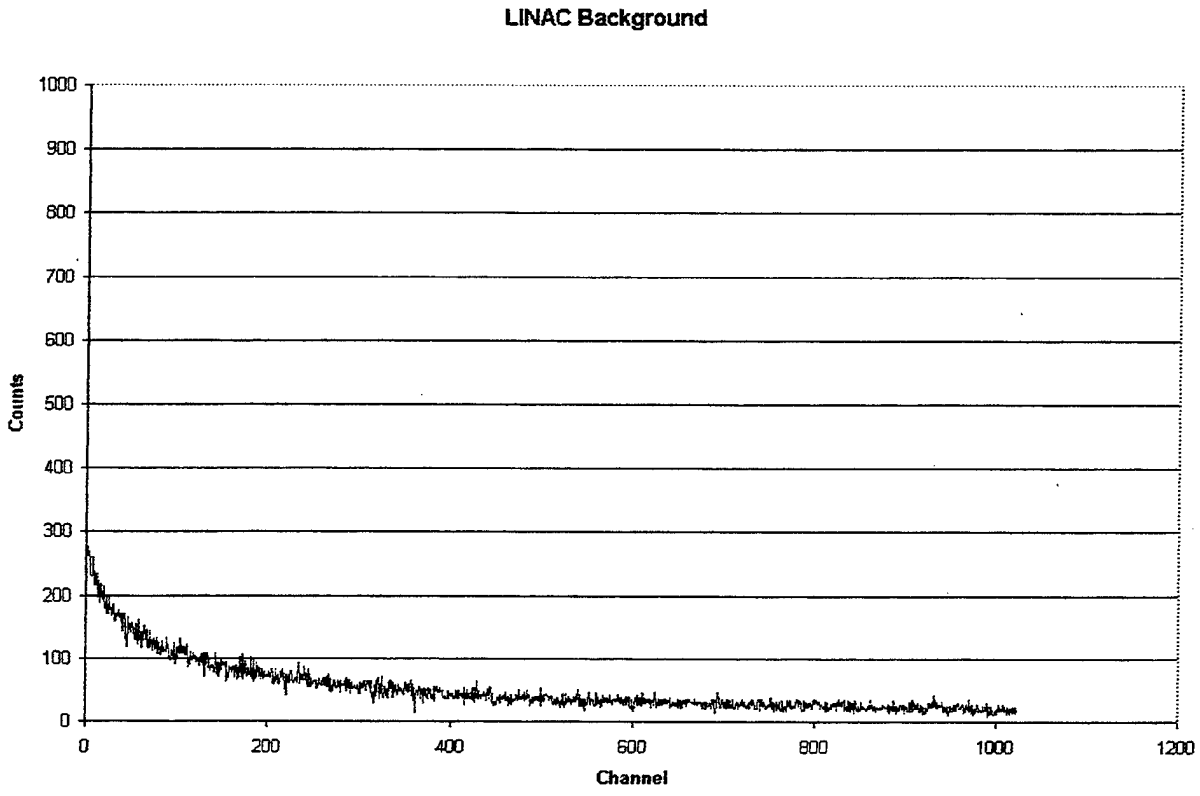

Figure 13. LINAC Background The collection time was 30 minutes. Channel 1000 corresponds to approximately 40 keV.

B. CHARACTERISTIC OR FLUORESCENT X-RAYS

If one considers the possibility that all the peaks in the Be PXR spectrum are characteristic or fluorescent x-rays, candidate elements for the 9.1 keV peak would be gallium (Ga) and germanium (Ge). Copper's 8.90 keV K_β emission might be considered a source of the 9.1 keV peak. Elements that might correspond to the 24.15 keV peak are indium (In) and tin (Sn) with K_α emission lines of 24.2 keV and 25.3 keV respectively.

Gallium, germanium and indium are far too rare to warrant serious consideration. Copper and tin were present in the target chamber as calibration sources. Both foils were positioned in the ladder approximately 10 cm below the beam during PXR collections. For the foils to produce characteristic x-rays, electrons would have to be scattered downward by the ladder or the crystal and then strike the foils. The resultant x-rays would then have to propagate to the detector through a cicuitous path. The same scenario holds true for fluorescent x-rays. The likelihood of either process being resposible for and of the peaks in the spectrum is low. In addition it is unlikely that copper's K_β emission would be present without its K_α emisssion.

Finally, the possibility that the target ladder might contain tin as an impurity or that fastners (screws etc.) might be comprised of tin must be considered. Tin's K_α emission line is 1.1 keV higher than the 24.2 keV peak. This is well within the energy resolution of the Si(Li) detector. In addition, previous experiments under the same conditions do not reveal the observed peaks. Extraneous characteristic or fluorescent x-rays can not explain the obsevered spectra.

C. RADIOACTIVITY IN THE ENDSTATION

It is conceivible that the LINAC end station has low levels of radioactivity. Energies for nuclear decay schemes, however, are in the hundreds of keV to MeV range and can be disregarded. The calibration source ^{113}Sn does have a K_α energy of 24.14 keV. However, care was taken to ensure that the radioactive sources were removed from the endstation after the static

calibration was completed eliminating this as a possiblity. To further substaniate this argument, since the ^{113}Sn source was not used as a static calibration source, it was never removed from the storage container. Therefore, if it were left in the endstation, then the other calibration sources would also be present. Other sources included ^{55}Fe, ^{109}Cd, and ^{137}Cs with energies of 5.9 keV, 22.1 keV, and 32.1 keV respectively. The ^{55}Fe and ^{109}Cd sources are more intense than ^{113}Sn, and their attenuation coefficients for dry air differ little from that of ^{113}Sn. As a result, peaks from these sources would also be present in the spectrum. Their absence from the spectrum eliminates the possibility that the 24.1 keV is attributed to ^{113}Sn. Therefore, radioactive sources in the end station does not explain the observed spectrum.

D. PXR FROM THE TARGET LADDER

If crystal planes from the aluminum in the ladder satisfied the Bragg relation, PXR might be produced if electrons from the beam were striking it. The beryllium crystal measured 4.5 mm in width. When the crystal was rotated as shown in Figure 14, the apparent width of the crystal is reduced to approximately 1.75 mm (4.5mm x sin 22.5°). The nominal diameter of the beam was 2 mm. In addition, to create a small beam a great deal of steering must be done with the end station steering magnets and focusing with the LINAC end station quadrupole magnets is also required. Past experience has shown that if the beam is not centered in the quadrupole magnets, the location of the beam changes with changes in the klystron frequency and phase. It proved impossible to center the beam in the quadrupoles while also achieving a small beam that passed through the geometric center of the target chamber. Therefore, it is assumed that a significant number of electrons were striking the ladder.

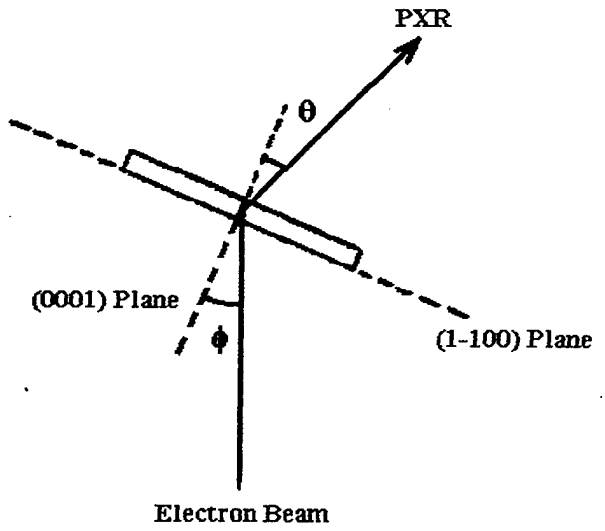

Figure 14. Relative Geometry of Electron Beam, Crystal, and PXR. $\phi = \theta = 22.5°$

Without prior knowledge of the orientation of the crystalline planes of the aluminum ladder it appears there are innumerable combinations of Bragg angle and planar spacing that may result in photon energies of 24.1 keV. Aluminum has a face-centered cubic crystalline cell with $\mathbf{a} = \mathbf{b} = \mathbf{c} = 4.05$ Å and $\alpha = \beta = \gamma = 90°$. Using this information, the number of possibilities can be reduced by considering the general form of the structure factor for FCC crystals. The structure factor is given by [Ref. 2]:

$$F = f[1 + e^{i\pi(h+k)} + e^{i\pi(h+l)} + e^{i\pi(k+l)}] \quad (2)$$

where f is the atomic scattering factor or form factor and h, k, and l are the Miller indices of the reflecting plane. Reflections that are necessarily absent occur when the Miller indices of the plane are mixed (odd and even integers) while those that are possible occur when the Miller indices of the plane are unmixed (all even or all odd integers). For x-rays reaching the detector, the Bragg angle of 22.5° still holds. Any other angle would not be within the field of view of the

detector. The 24.15 keV peak corresponds to x-rays with a wavelength of 0.5 Å. Finally, the interplanar spacing of a cubic crystal can be derived through the use of the lattice constants (**a**,**b**,**c**,α,β,γ) as a function of the Miller indices of the plane [Ref. 2]. It is given by:

$$d_{hkl} = \frac{a}{\sqrt{h^2 + k^2 + l^2}} \tag{3}$$

Applying Bragg's law to the required angle and wavelength requires that d_{hkl} equal 0.65 Å. Substituting this into equation (3) and solving for the Miller indices gives the following:

$$d_{hkl} = 0.65 \text{ Å requires } h^2 + k^2 + l^2 = 38.8 \tag{4}$$

By trial and error, indices may be chosen, the sum of who's squares total approximately 38. Using equation (4) , the plane (442) gives $h^2 + k^2 + l^2 = 36$. Applying equation (3) and then equation (1) gives an energy of 23.9 keV. If this is considered a second order reflection, then the first order plane is (221) which is necessarily absent according to equation (2). This, then, offers a possible explanation of the 24.15 keV peak if the 9.1 keV peak is considered to result from the (0002) plane of the Be crystal. However, past PXR experiments have observed x-ray spectrum from electrons incident on the aluminum target ladder and have not seen any structure neart 24 keV. In order for aluminum to be the source of a 24.15 keV peak, it must have the proper crystal orientation. It is highly unlikely that commerical grade aluminum would be oriented at the kinematic conditions necessary, therefore, PXR from the aluminum ladder is improbable.

E. OTHER COHERENT X-RAY PROCESSES

The shape of the 24.15 keV peak implies that it is the result of some discrete (quantum mechanical) processes or x-ray diffraction phenomenon. Other coherent x-ray processes that may be considered are transition radiation, coherent bremsstrahlung and, channeling radiaton. All three are emmitted into a cone within an angle $\phi \sim \gamma^{-1}$ relative to the velocity vector of the

incident electron. Since the x-rays from each process must arrive at the Si(Li) detector diffration must be taking place and the Bragg relation must hold. Therefore, regardless of the energy of the photons created by each process, only those with wavelength equal to 1.3 Å and energy equal to 9.1 keV will arrive at the detector. The 24.15 keV peak can not be accounted for by these processes.

F. GEOMETRY CONSIDRATIONS

The argument that the wrong crystal planes were being used to calculate the expected PXR energy has two problems. First, if PXR was being generated from the (1-100) plane and those planes that are parallel with it, the 9.1 keV peak can not be PXR and an alternate explanation for its presence must be found. However, when the crsytal was "rocked" to determine the best alignment of the experiment for PXR, the 9.1 keV peak showed a strong angular dependence. This can be seen in the spectra contained in the appendix. Based on the data sheet provided by the manufacturer, theoretical calculations that predict a 9.1 keV PXR peak and its strong angular dependence, the 9.1 keV peak is most certainly PXR from beryllium.

A second problem with this explanation is that additional peaks are missing from the spectrum. The geometry depicted in figure (2b) indicates that peaks with energies of approximately 6 keV, 12 keV and 24 keV are expected. Missing reflections can be predicted by determining the structure factor, |F|, of the unit cell of a crystal.

The unit cell of a HCP crystal contains two atoms. One located at 0 0 0 and the other at 1/3 2/3 1/2. The structure factor for this crystal then is given by [Ref. 2]:

$$F = f[e^{2\pi i(0)} + e^{2\pi i(h/3+2k/3+1/2)}] \qquad (5)$$

When |F| = 0, the reflection from that plane is necessarily abscent. Because the structure factor of beryllium contains fractions (h, k, and l are always integers) we mutilply equation (5) by its complex conjugate to get a real result. Thus, |F| for beryllium and other HCP crystals becomes:

$$|F|^2 = 4f^2 \cos^2 \pi(\tfrac{h+2k}{3} + \tfrac{l}{2}) \qquad (6)$$

It is obvious that for the structure factor to be zero, h+2k must be zero or a multiple of three and l must be odd. Because the planes shown in figure (2b) do not intercept the **c** axis, l = 0 for all three planes. It is therefore impossible to make $|F|^2 = 0$ and higher order reflections are allowed. Atomic scattering factors for the three planes shown in figure (2b) range from 1.9 to 1.6 while the argument of the cosine is $\pi/3$ or some integral multiple of $\pi/3$. The structure factor for each plane, then, is roughly equal, and therefore the expected intensity of the "reflected" photons is the same for each. Structure factor calcultions for the "C" plane show that the first order reflection with an expected energy of 4.5 keV is necessarily abscent:

$$|F|^2 = 4f^2 \cos^2 \pi(\tfrac{0+0}{3} + \tfrac{1}{2}) = 0 \qquad (7)$$

However, reflections from the (0002) plane are possible and give an energy of 9.1 keV. Since the second order reflecting plane for 9.1 keV can be rewritten after a translation of the axis as (0001), an 18 keV peak is not expected. This is in agreement with the spectrum and further substantiates the argument that the Bragg relation was satisfied for the geometry of Figure 3(c) and Figure 3(d).

G. GROWTH AND DEFORMATION FAULTS

Faults can result in the (0002) planes of HCP crystal as the result of improper crystal growth or crystal deformation resulting from applied stresses. The result is that the normal ABAB

sequence that categorizes a crystal as HCP incurs short-range changes to, for instance, ABABCBCBABAB or ABABCACACABAB.

To help visualize this, Figure 15(a-e) depicts the relationship of the atoms in the "A", "B", and "C" stacking patterns. Additionally, Figure 15(d) shows a normal AB sequence while Figure 15(e) shows a BC sequence. Note that the only difference between "B" and "C" is a 60° rotation of the atoms. Thus, an AC fault looks much the same as Figure 15(d) except the layer "B" is replaced by "C". The ACAC pattern is repeated several times until the fault ends. The same is true of BCBC pattern. Several layers follow the BC sequence before an "A" layer occurs to restart the proper sequence.

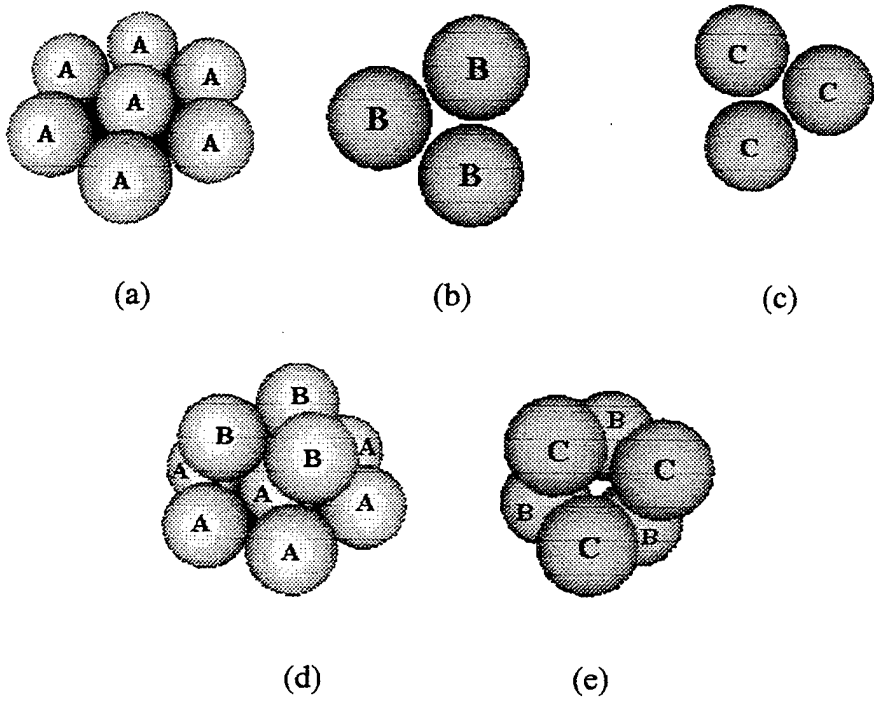

Figure 15. (a) Arrangement of atoms in "A" layer. (b) Arrangement of atoms in "B" layer. (c) Arrangement of atoms in "C" layer. (d) Normal HCP "AB" stacking pattern. (e) A "BC" growth or deformation fault.

It is obvious from this discussion that growth and deformation faults do not affect the spacing of the (0002) planes and therefore do not affect the energy of PXR reflections. Instead, growth and deformation faults affect the density of atoms at points in the crystal. The result is a broadening of the peak and a reduction in intensity rather than the appearance of new PXR peaks. [Ref. 8]. Growth and deformation faults can not explain the observed spectrum.

Consequently, none of the possibilities for explaining the unexpected observations provides an adequate source for the spectra seen. We must conclude that this experiment is observing a previously unobserved phenomenon.

V. THEORETICAL BACKGROUND

A. PXR THEORY

Feranchuck and Ivanshin proposed the first theory of PXR in 1983. Using the language of Quantum Electrodynamics, the electric field of a relativistic electron interacting with the atomic planes of a crystal can represented as the superposition of a cloud of virtual photons. In explaining the phenomenon, then, we can replace the beam of electrons with a beam of virtual photons. Those virtual photons that satisfy the Bragg condition are scattered by the crystal planes and manifest themselves as real photons in the form of x-radiation.

Feranchuck and Ivanshin expressed the spectral and angular distribution of the radiation by:

$$\frac{\partial^2 N}{\partial n_\perp \partial \omega} = \frac{e^2}{2\pi}\omega L_a |g_\tau|^2 \frac{\left|\kappa_\perp, \omega v + \tau^2\right|}{\left[(\kappa_\perp - \tau_\perp)^2 + \frac{\omega^2}{v^2}\left(1 - v^2\right)\right]^2}\left[1 - e^{\frac{-L}{L_a}}\right]\delta(q) \tag{8}$$

where

$$q = \frac{\omega}{v} - \sqrt{\omega^2 - \kappa^2} + \tau_z - \frac{\omega}{2}\left[\mathrm{Re}(g_0) - \theta_s\right] \tag{9}$$

N is the number of photons per electron. e is the electron charge, and θ is the multiple scattering angle. g_0 and g_τ are the perpendicular and parallel Fourier components of the dielectric susceptibility. τ is the reciprocal lattice vector with components τ_x, τ_y, τ_z. $\tau_\perp$ is the component perpendicular to v, the particle velocity. $n_\perp$ is the photon index of refraction. ω is the frequency of the emitted photon. $\kappa_\perp$ is the component of the wave vector of the emitted radiation perpendicular to the crystal plane. Equation (8) is written in a reference frame whose z-axis is aligned with the incident particle's velocity. L is the crystal thickness, and the photon absorption length $L_a = [\omega \cdot \mathrm{Im}(g_0)]^{-1}$. Equation (8) indicates that the angular distribution of PXR consists of a

series of peaks in energy centered on the Bragg angle (θ_B). The frequency of PXR is concentrated near ω_B which is:

$$\omega_B = \frac{\tau}{2\sin\theta_B} \tag{10}$$

Thus, PXR depends on the crystal structure and the angle between v and the crystal planes and is independent of the electron's energy. PXR intensity is proportional to $|g_\tau|^2$ and therefore is largest in those crystals where the density of the atoms is a maximum.

The number of photons per electron per solid angle per electron energy can be found using angular displacement resulting in [Ref. 1]:

$$\frac{\partial^3 N}{\partial\theta_x\partial\theta_y\partial\omega} = \frac{1}{2\pi^2}\frac{e^2}{\hbar c}\frac{1}{\omega_B}|g_\tau|^2 \frac{\theta_x^2\cos^2(\theta_B)+\theta_y^2}{(\gamma^{-2}+\theta_x^2+\theta_y^2+|g_0|)16\sin^4\theta_B(\frac{\theta_x}{\tan\theta_B}-\frac{\Delta\omega}{\omega_B})^2+\rho_s^2} \tag{11}$$

θ_x and θ_y represent the angular displacement from the Bragg condition. $\rho_s \equiv \lambda/[L_a(\omega)2\pi]$ with $L_a(\omega)$ defined as the absorption length of the emitted photon. $\gamma = [1-(v/c)^2]^{-1/2}$. ω_B is the photon frequency at the Bragg condition and $\Delta\omega = \omega - \omega_B$.

Finite detector aperture must also be considered in PXR experiments. There are two regimes that must be considered. These are referred to as the narrow line limit and the aperture limited bandwidth regimes. The narrow line limit is characterized by $\Delta\theta_x \cong \rho_s$. This thesis was conducted in the aperture limited bandwidth regime where $\Delta\theta_x >> \rho_s$. If equation (11) is integrated over the solid angle viewed by the detector, the spectral distribution can be approximated by [Ref. 3]:

$$\frac{\partial N}{\partial \omega} \propto \begin{cases} \Delta\theta_x J_2(u), & -\overline{\theta_x} < \theta_x < \overline{\theta_x} \\ 0, & \text{otherwise} \end{cases} \tag{12}$$

where,

$$J_2(u) = \cos^2(2\theta_B)u^2\left[\frac{\alpha_y}{1+u^2}\frac{1}{\alpha_y^2+1+u^2} + \tan^{-1}\left(\frac{\alpha_y}{1+u^2}\right)\left(\frac{1}{1+u^2}\right)^{3/2}\right] + \left[\tan^{-1}\left(\frac{\alpha_y}{(1+u^2)^{1/2}}\right)\frac{1}{(1+u^2)^{1/2}} - \frac{\alpha_y}{\alpha_y+1+u^2}\right] \tag{13}$$

and,

$$u = \tan\theta_B \frac{(\omega-\omega_B)}{\omega_B\theta_{ph}} \tag{14}$$

Here $\alpha_y = \theta_y/\theta_{ph}$. θ_{ph} is the characteristic angular spread of the PXR and is dependent on the structure of the crystal and the divergence of the incident particles. In this regime, the bandwidth of the energy is based on the value of $\Delta\theta_x$ and the full width half maximum of $J_2(u)$ and is referred to as the "near field" region. If $\Delta\theta_x$ is less than $J_2(u)$, then the energy bandwidth is proportional to $\Delta\theta_x$ and $J_2(u)$ plays little role. This regime is referred to as the "far field" regime and is the area of interest for this thesis. As can be seen from Figure 16 and Figure 17 [Ref. 3], much of the PXR radiation is outside the field of view of the detector for the "far field" as compared to the "near field."

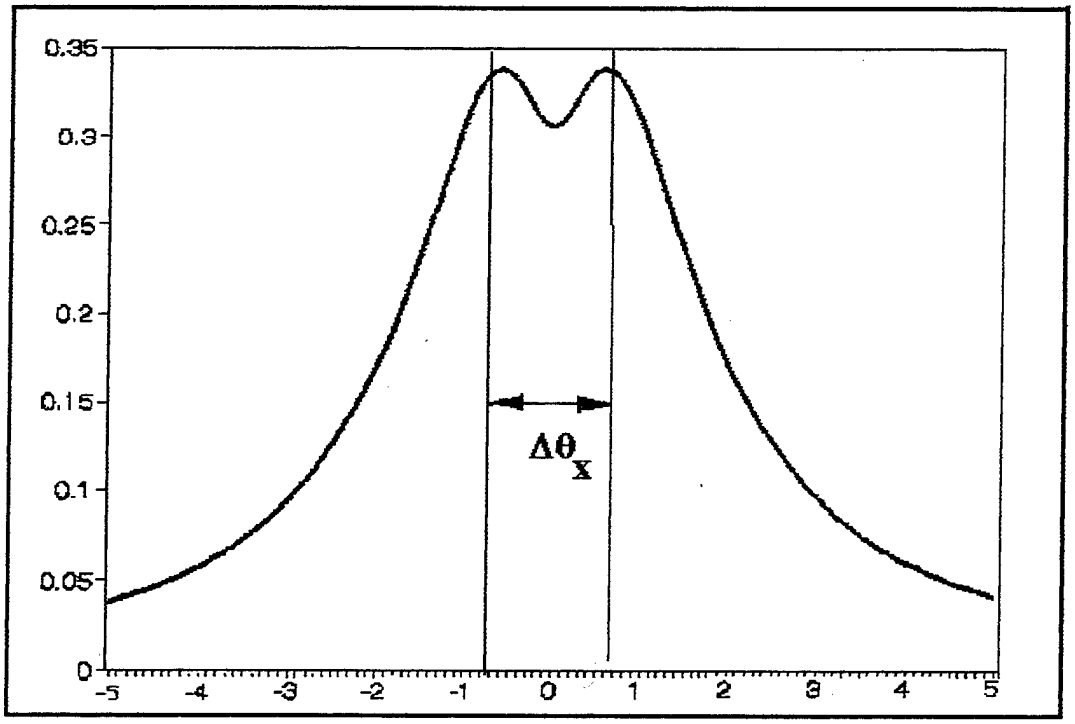

Figure 16 - J_2 and the Field of View for the "Near Field" Regime

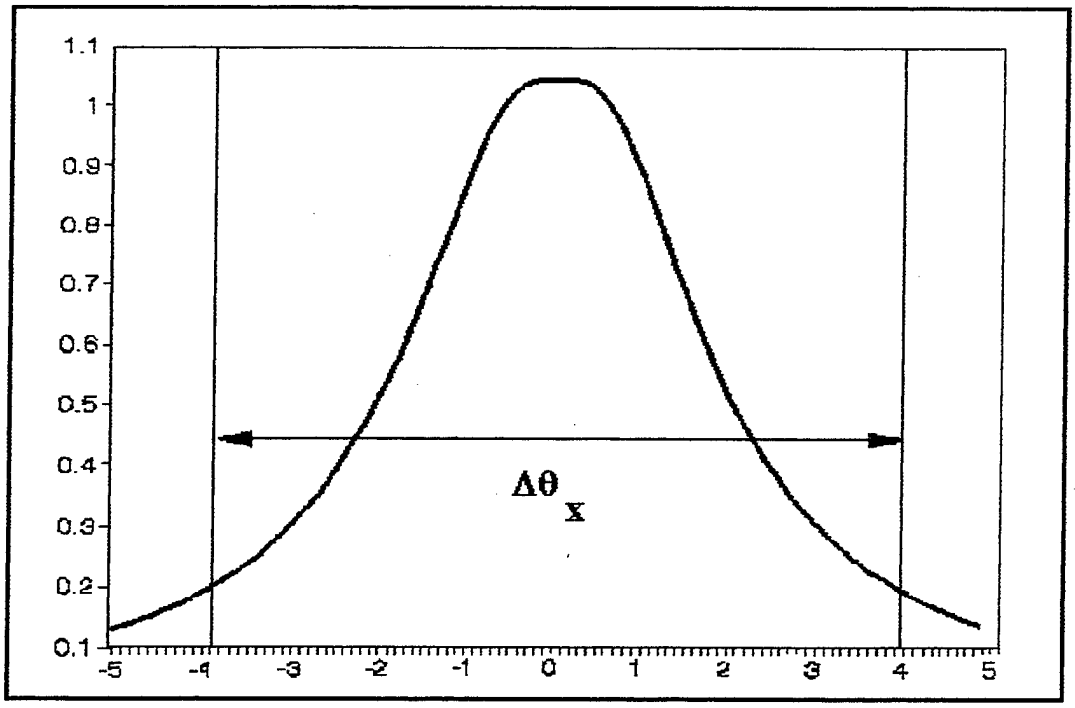

Figure 17 - J_2 and Field of View for the "Near Field" Regime

B. $P_{CRYSTAL}$ THEORY

Freudenberger starts from the double differential cross section for PXR [Ref. 6]:

$$\frac{d^2\sigma_{atom}^{PXR}}{dEd\Omega} = 8\pi\alpha^3\lambda\!\!\!^{-2}V_c\sum_{\vec{n},\sigma}\frac{|S_N F|^2 f^2}{(c-\vec{n}\cdot\hat{k})\omega n}\left|\frac{\vec{e}_{\vec{k},\sigma}(n\omega\vec{v}-\vec{g}c^2)c}{c^2(\vec{k}+\vec{g})^2-n^2\omega^2}\right|^2\delta(E-E_{PXR}) \qquad (15)$$

S_N is the structure normalized to the crystal volume V_c of the unit cell. F is the atomic form factor, f the Debye-Waller factor, α the fine structure constant, E the photon energy, $\vec{e}_{\vec{k},\sigma}$ the polarization vectors, ω the radiation frequency, $\vec{v}$ the electron velocity, and $\vec{g}$ the reciprocal lattice vector. $\lambda\!\!\!^{-} = \lambda/2\pi$. λ is the wavelength of the emitted photon, and $\vec{k}$ the direction of photon observation. E_{PXR} is given by [Ref. 6] as:

$$E_{PXR} = \hbar c\frac{\vec{g}\cdot\vec{v}}{c-n\vec{v}\cdot\hat{k}} \qquad (16)$$

Equation (15) represents the double differential cross section for the emission of a single photon into the energy interval dE and the solid angle $d\Omega$ per unit cell of the crystal. From equation (15), at low electron energies, the intensity of PXR radiation, $P_{Crystal}$, depends on the properties of the crystal and can be approximated by [Ref. 6]:

$$\frac{|S_N\cdot F|^2 f^2}{g^3}L_{abs} \approx \frac{dN}{d\Omega} \equiv P_{Crystal} \qquad (17)$$

L_{abs} is the photon absorption length. Freudenberger has further simplified equation (17) by assuming that the crystal properties are proportional to atomic number of the crystal [Ref. 9] and expressed this as:

$$P_{crystal} \approx \frac{z^2}{\sigma_{abs}} \qquad (15)$$

where z is the atomic number and σ_{abs} is the cross section for x-ray absorption. $P_{crystal}$ is shown in Figure 18 for an energy of 20 keV. Beryllium (Z=4) is predicted to be the best PXR radiator at 20 keV since its absorption cross section is small.

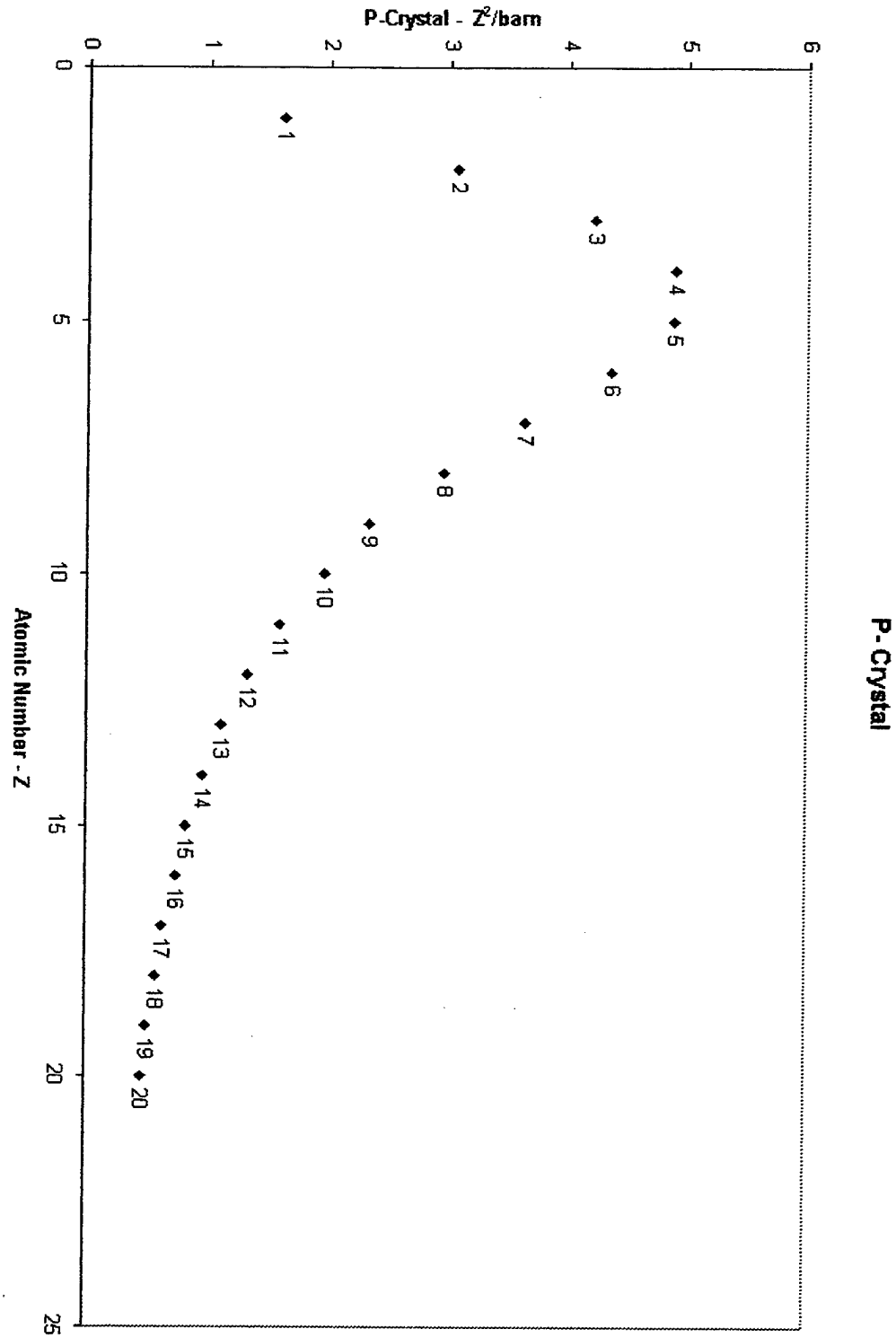

Figure 18. The relative intensity of PXR radaition, $P_{Crystal}$, at 20 keV plotted for various atom numbers (Z). Beryllium and boron are predicted to be the most efficient PXR radiators in the 20 keV regime.

THIS PAGE INTENTIONALLY LEFT BLANK

VI. CONCLUSIONS

This thesis has established a foundation of understanding that will aid in future PXR experiments with beryllium crystals. The observed spectrum is not expected from current theory. Possible explanations for the observed peaks are presented, but are shown to be insufficient explanations for the observations. Several things warrant further experiment.

First, spectra should be collected to further study the 24.15 keV peak. The only possible explanation as presented is PXR from the aluminum target ladder, but the circumstances which would give a peak structure at that energy is highly improbable. To eliminate problems of electron scattering by the ladder either a larger crystal will be needed or a better means of mounting the crystal needs to be devised. The manufacturer of the crystal, MaTecK of Jülich, Germany, experienced difficulties in manufacturing the crystal, which delayed its arrival. Additionally, the small crystal size that was used cost $1650. A larger crystal may prove even more difficult to manufacture and will surely be more expensive.

The experiment conducted for this thesis has only explored generation of PXR from the (0002) plane. In order to obtain x-ray energies of interest for mammography, PXR from the (1-100) plane and those planes parallel with it (Figure 3(b)) should also be explored. The possibility of a first order energy peak at 24 keV that is further enhanced by higher order peaks from the 8 keV and 12 keV reflections may provide PXR intensities high enough for mammography and a wide variety of applications.

Finally, PXR photon yield per electron must be determined. The experiment conducted for this thesis was curtailed due to the flooding in Halligan Hall.

This thesis observed a previously unmeasured PXR spectrum from beryllium. The spectrum is in variance with theoretical predictions. This experiment provides a challenge for

further experimentation and theoretical work. This thesis considered several possibilities to explain the observed spectrum, but all have proved inadequate.

APPENDIX A. PXR SPECTRA MEASURED FOR BERYLLIUM CRYSTAL

Figure Number	Date	Collection Time (Seconds)	Bragg Angle (Deg)	Peaks (keV)	Notes
19	12/04/98	915	17.0	N/A	
20	12/04/98	936	18.0	8.9	
21	12/04/99	609	18.5	9.2	Peak broader
22	12/04/99	704	20.0	9.1	
23	12/04/99	323	20.2	9.2	Weak/Broad
24	12/09/99	900	17.0	N/A	
25	12/09/99	900	17.5	N/A	
26	12/09/99	900	18.0	9.23	Very broad
27	12/09/99	900	18.5	N/A	Peak disappears
28	12/09/99	1000	19.0	9.5	Very broad
29	12/09/99	908	19.5	9.38	Sharp
30	12/09/99	1613	19.5	9.2	Collection extended for better statistics
31	12/09/99	8845	19.5	8.9	Collection extended for better statistics
32	12/11/99	900	19.5	9.2 24.5	Tilt = 0; 24.5 keV peak evident early
33	12/11/99	900	19.5	9.2	Tilt = 1.1; 24.5 keV peak no longer evident
34	12/11/99	901	19.5	9.3	Tilt 2.2
35	12/11/99	900	19.5	9.2	Tilt = 3.3; Peak sharp
36	12/11/99	904	19.5	9.25	Tilt = 4.4
37	12/11/99	902	19.5	9.28	Tilt = 5.5
38	12/11/99	900	19.5	9.17	Tilt = 6.6; Peak broad
39	12/11/99	908	19.5	10.5	Tilt = 7.7; Peak moved to 10.5 keV; broader
40	12/15/99	12000	19.5	8.18 9.1 24.15	Extended collection time. Corrected for detector efficiency and background removed

Table 2. Summary of PXR Spectra. Figures 19-31 are "rocking curve" spectra. Figures 32-39 investigated the optimal tilt angle of the crystal. Figure 40 is the extended PXR collection.

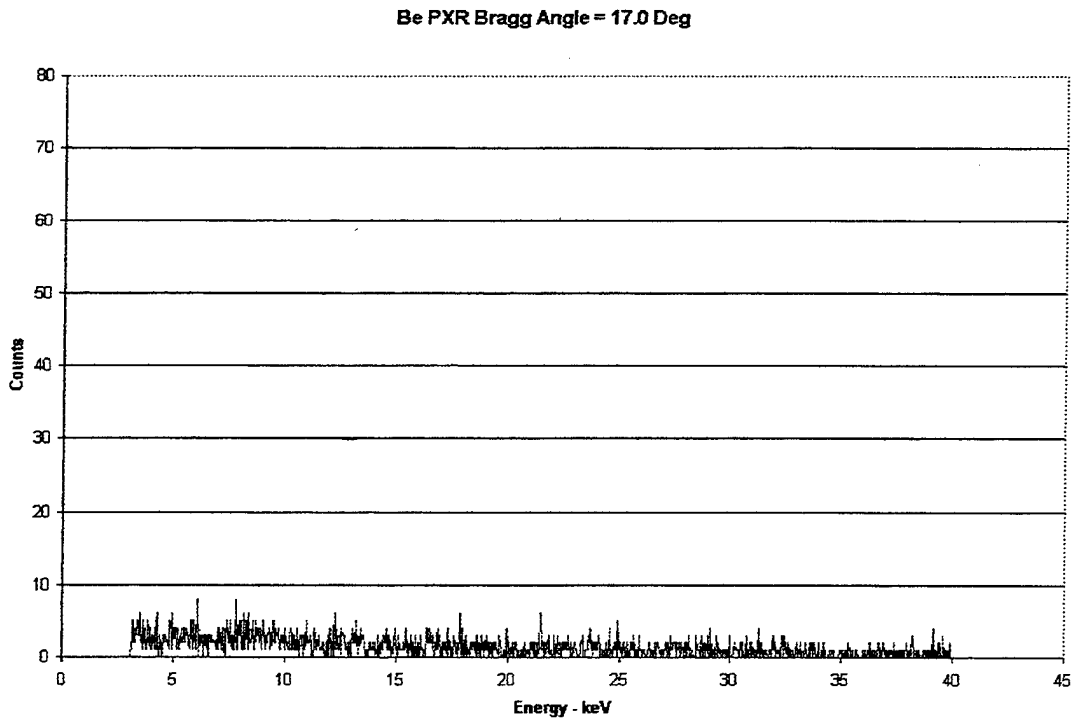

Figure 19

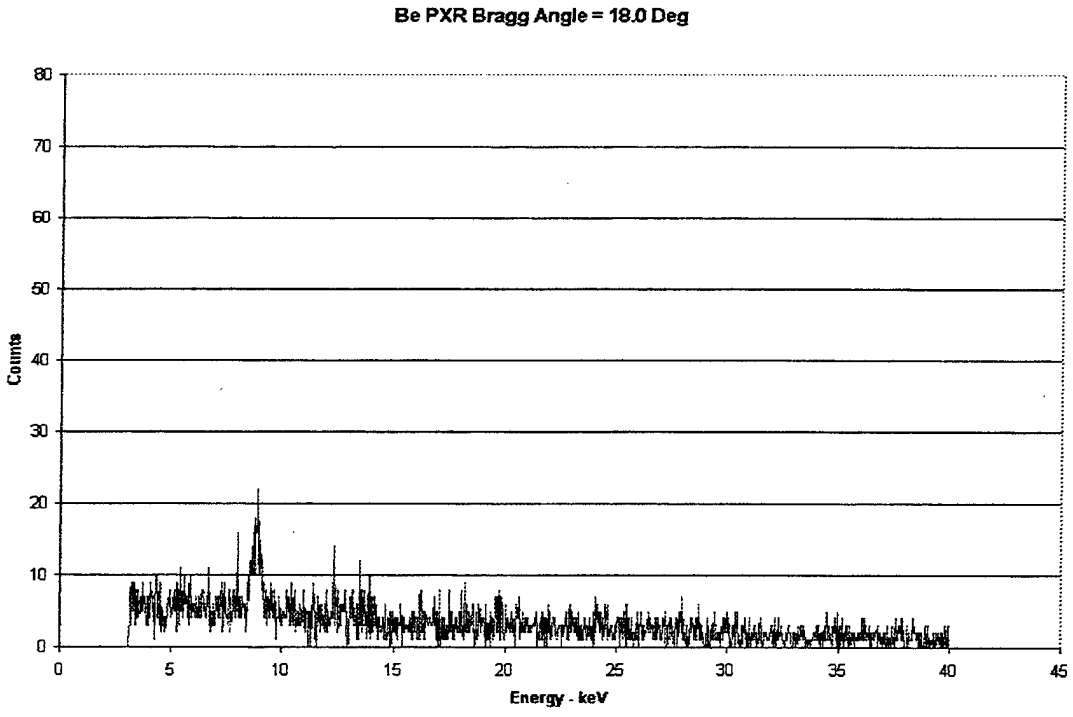

Figure 20

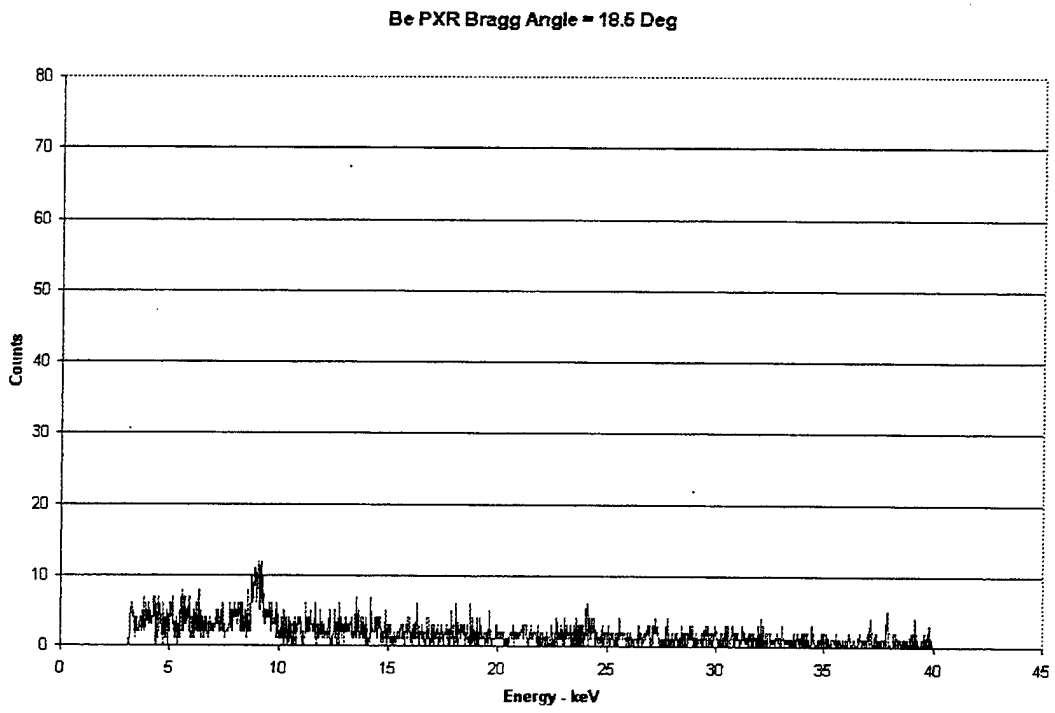

Figure 21

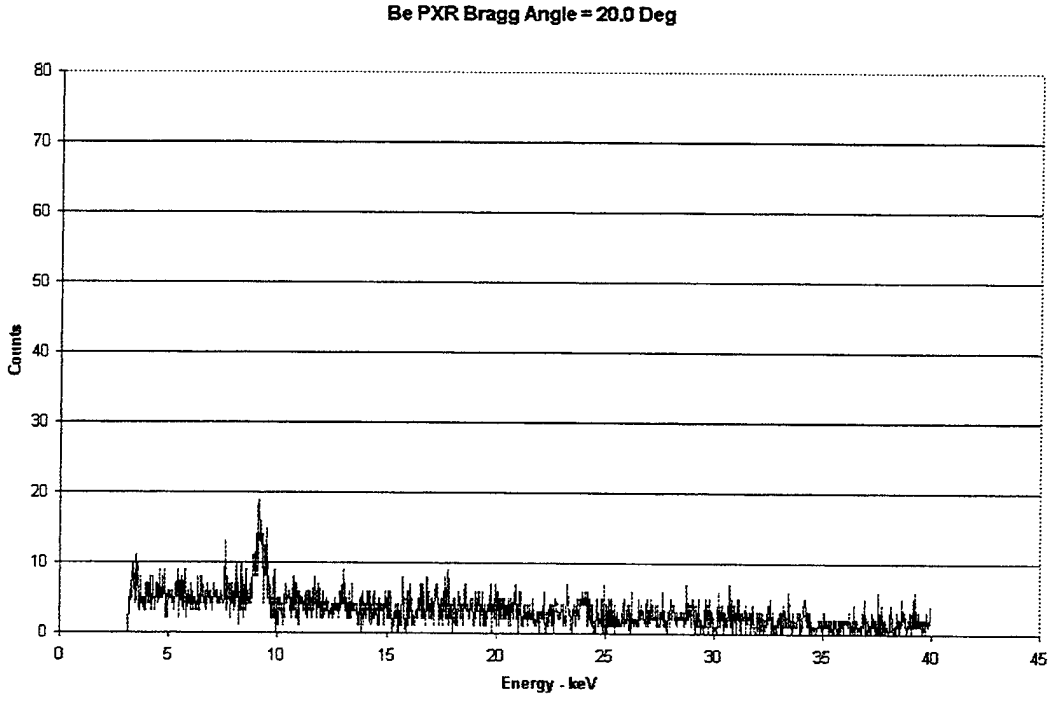

Figure 22

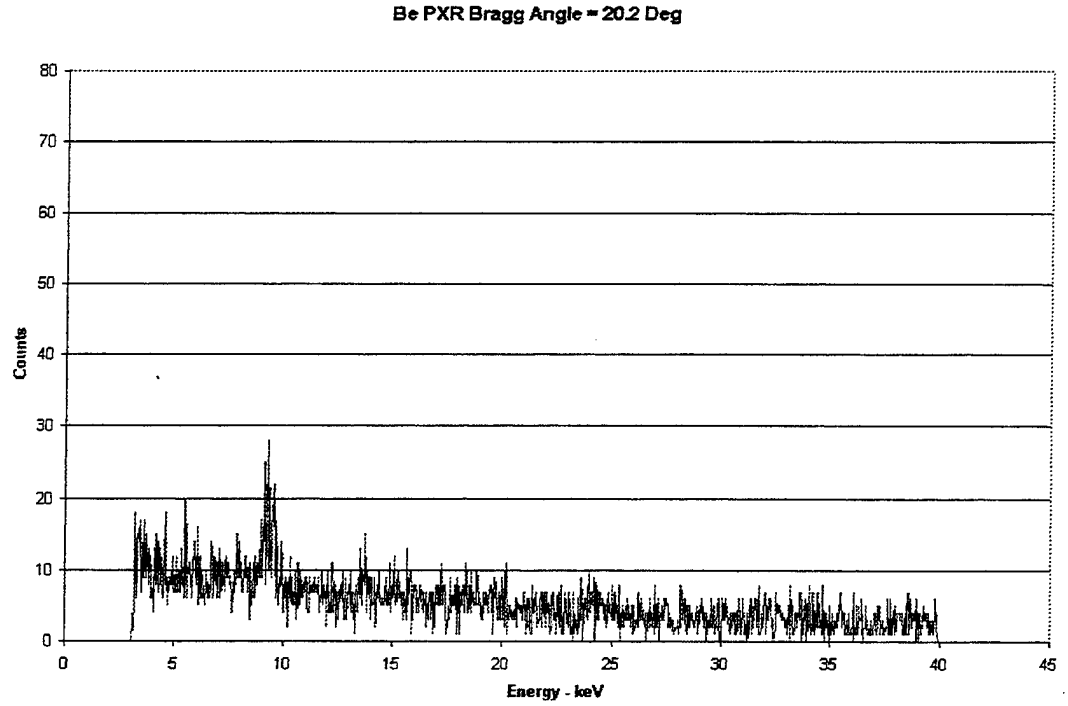

Figure 23

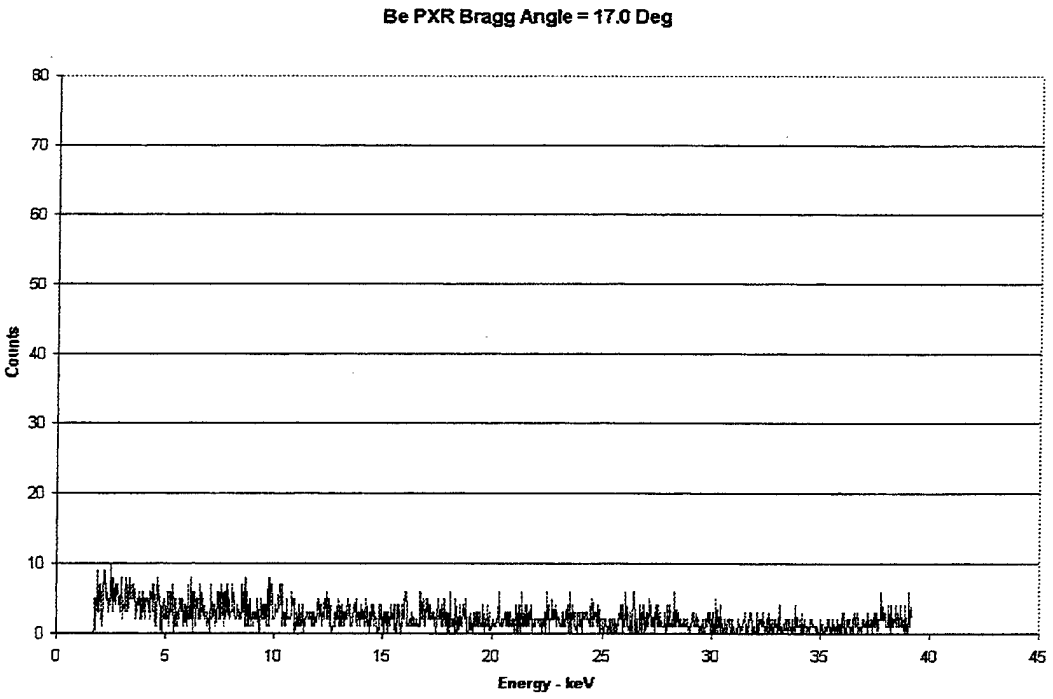

Figure 24

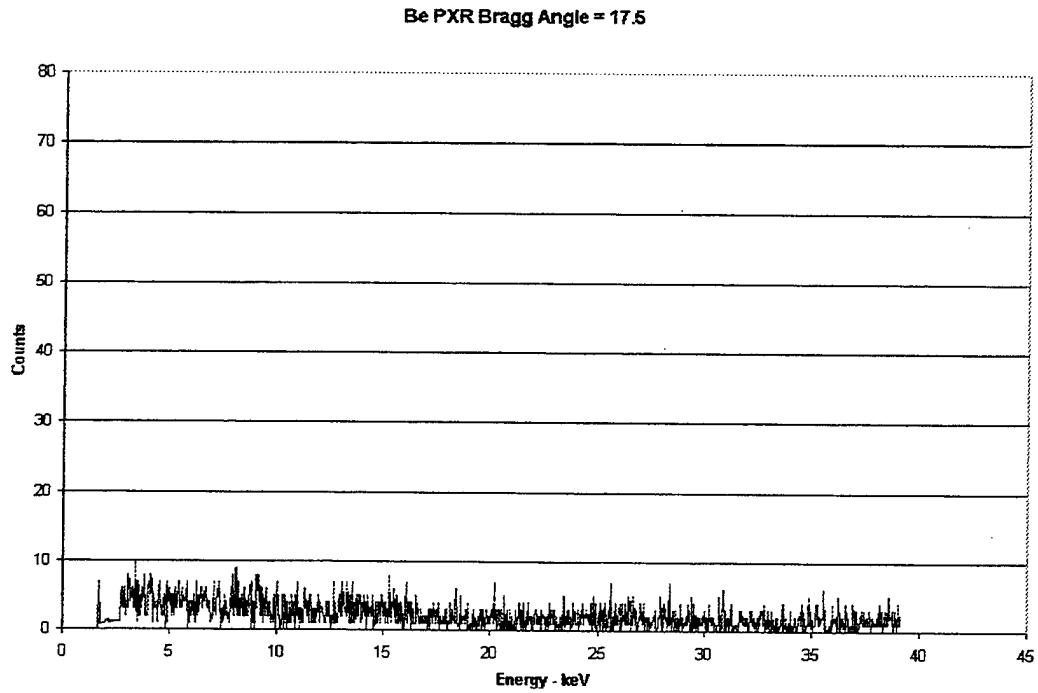

Figure 25

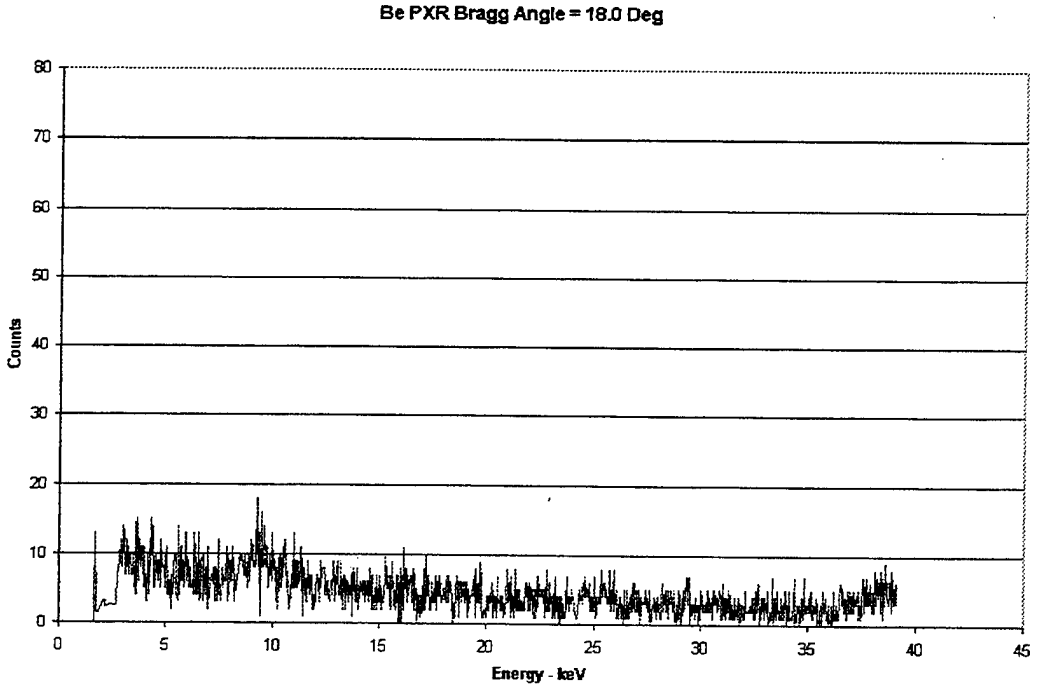

Figure 26

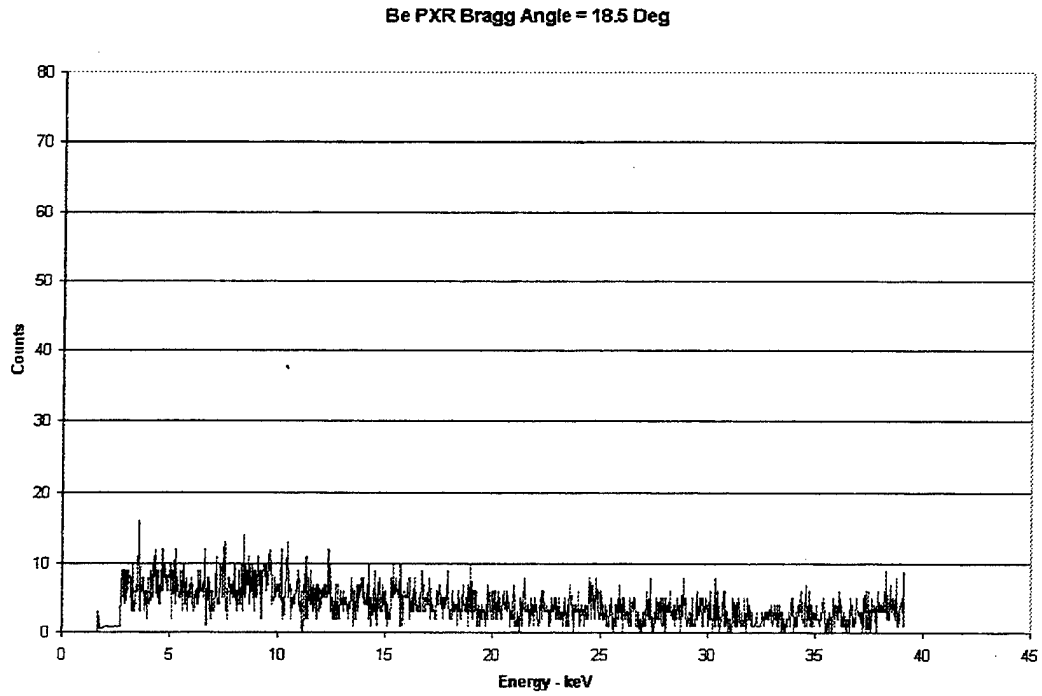

Figure 27

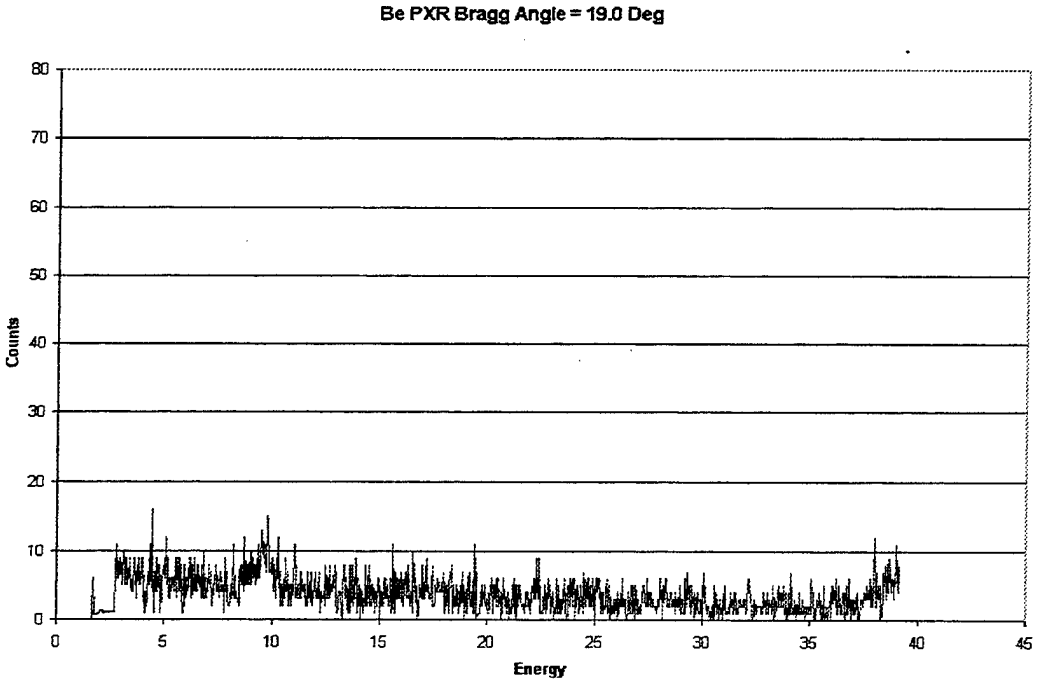

Figure 28

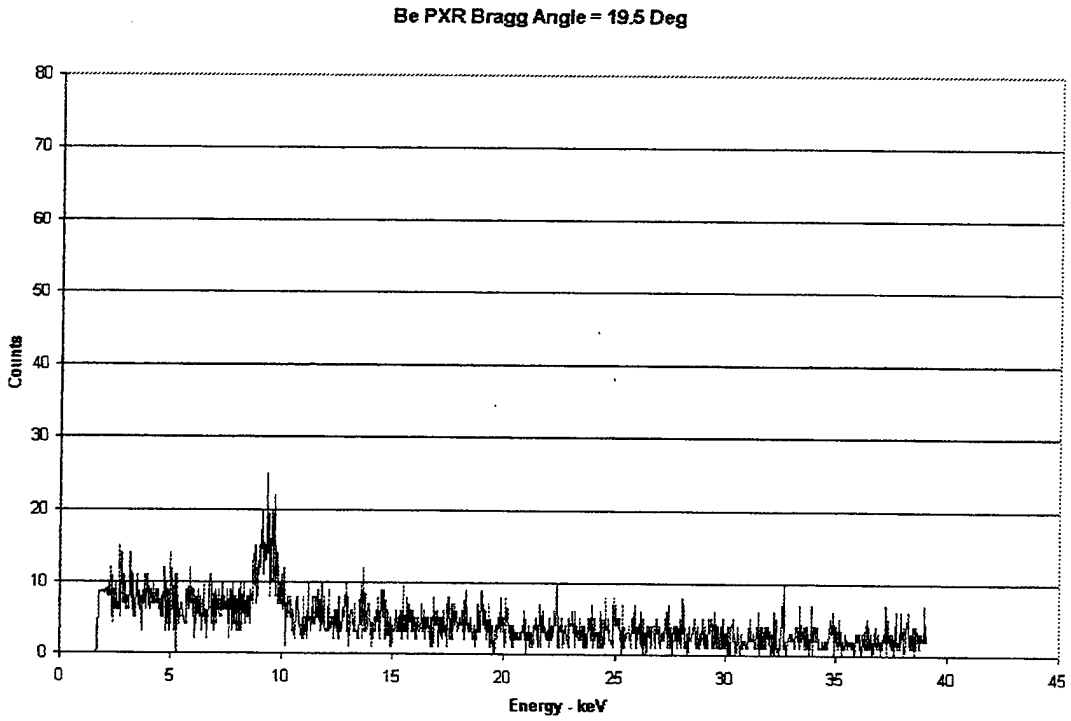

Figure 29

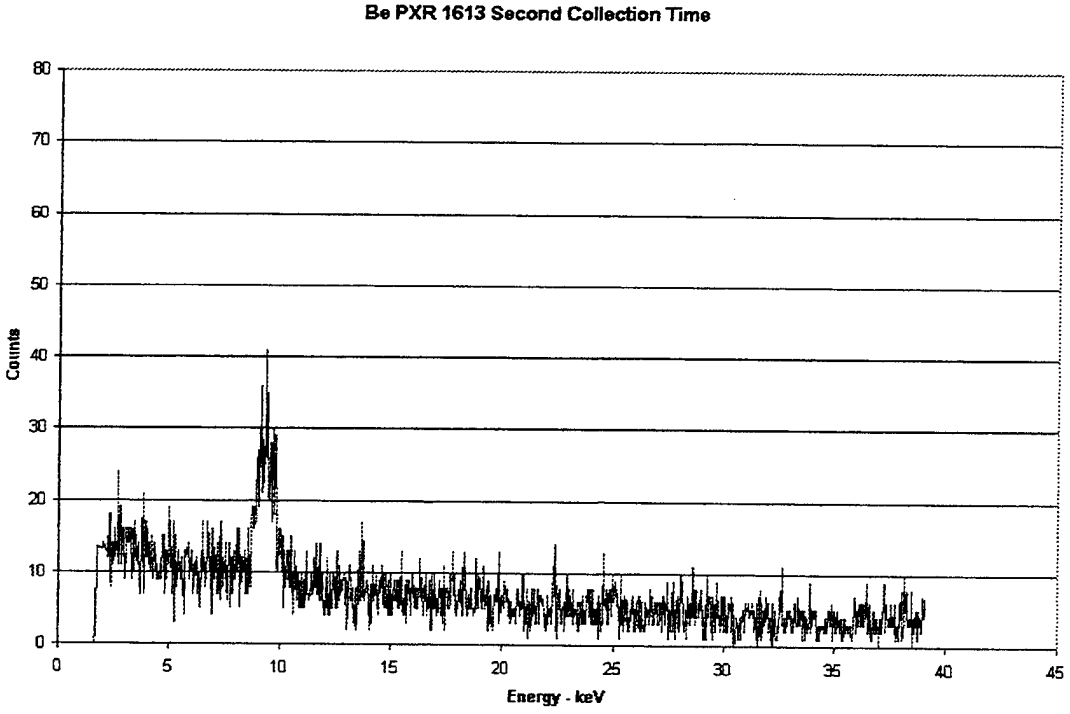

Figure 30

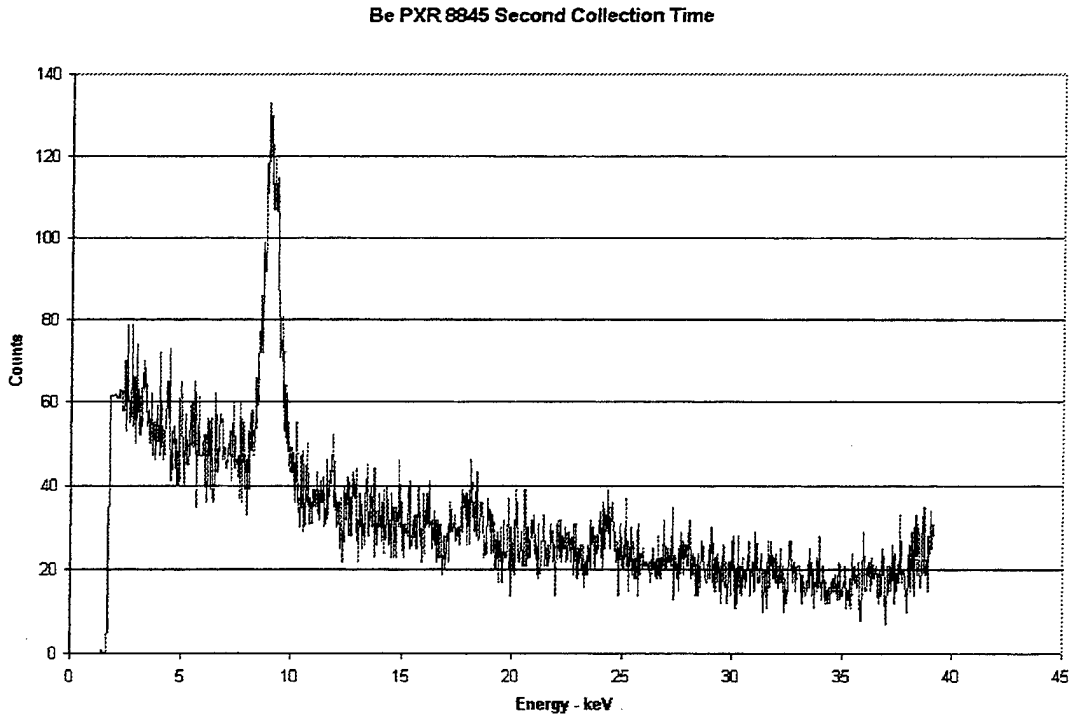

Figure 31

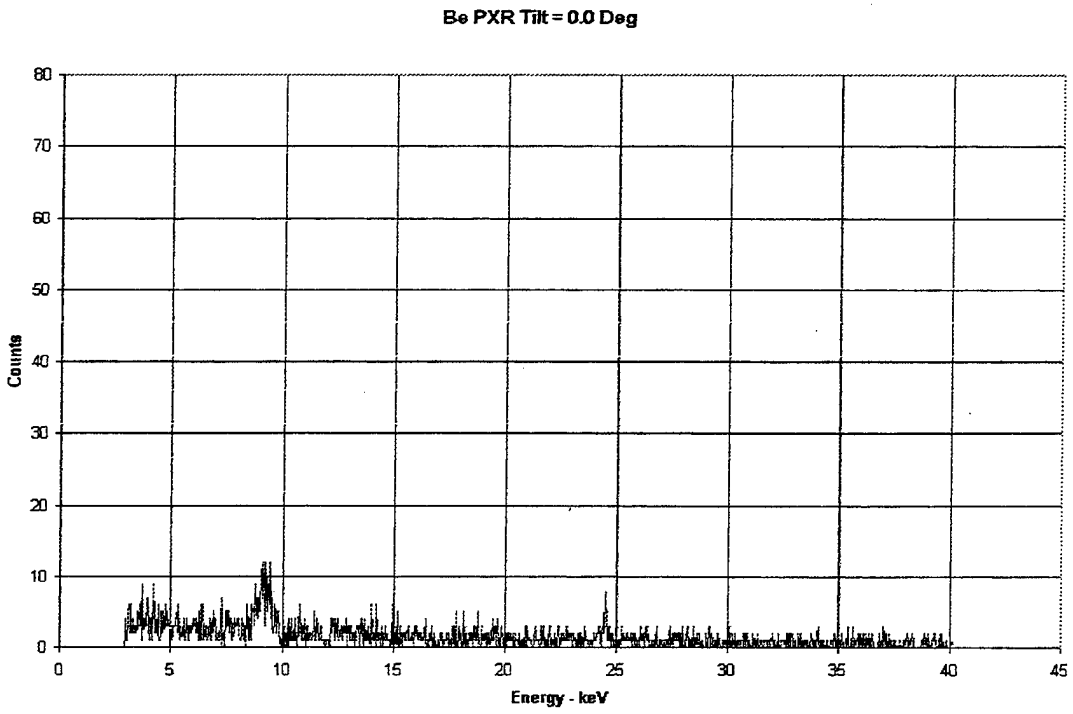

Figure 32

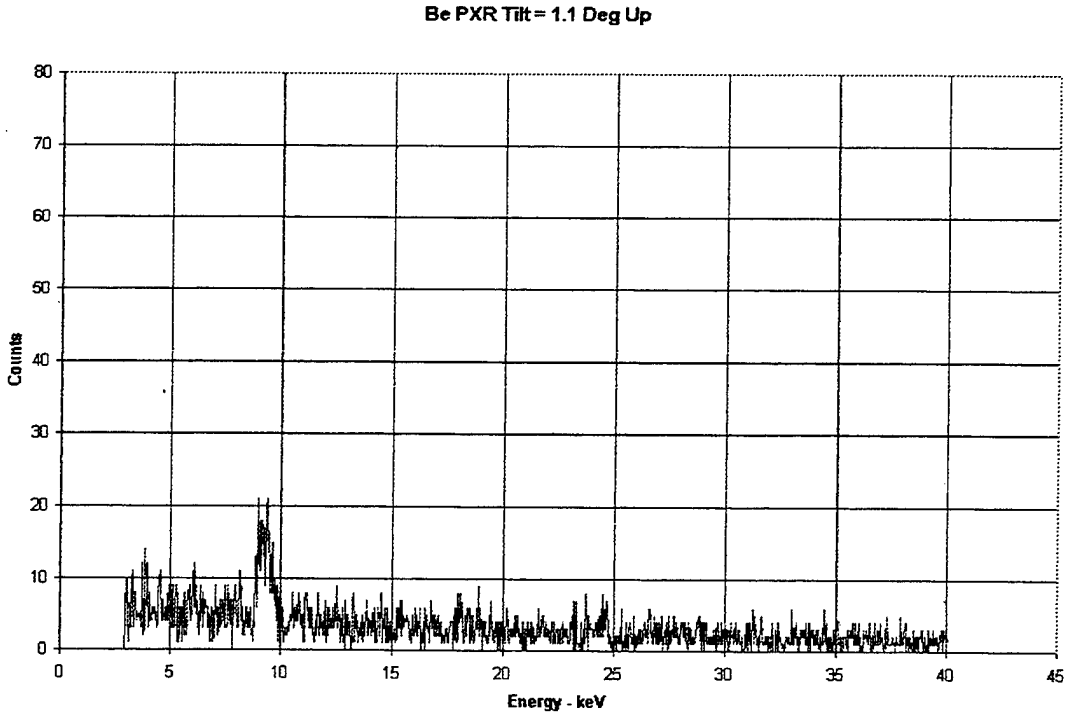

Figure 33

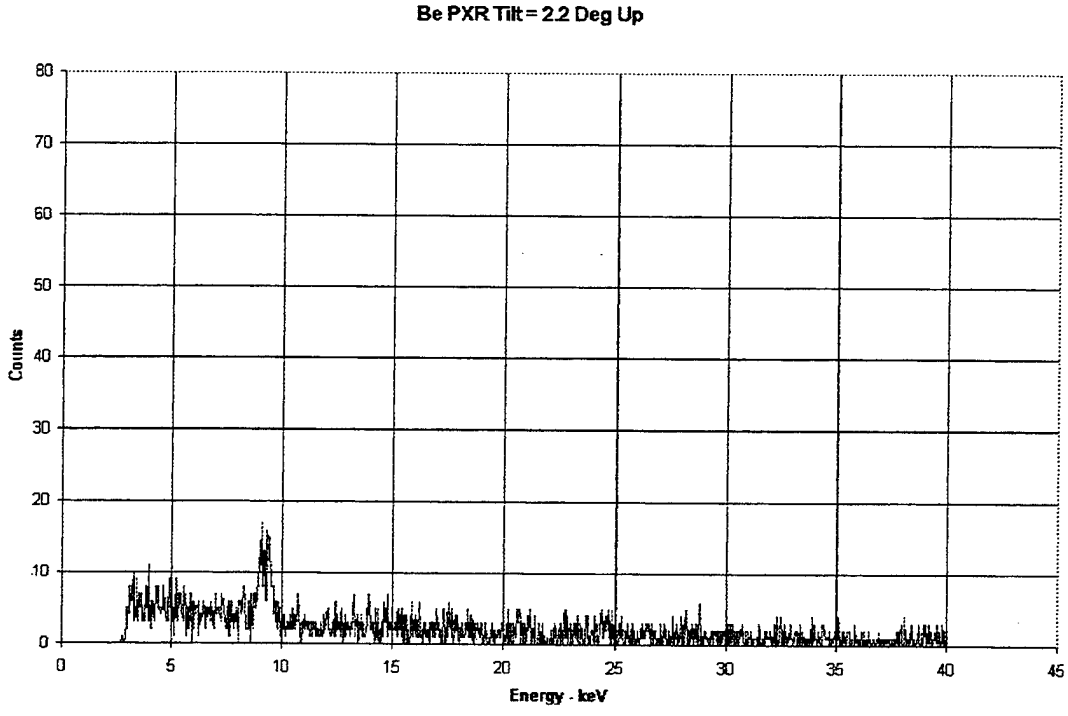

Figure 34

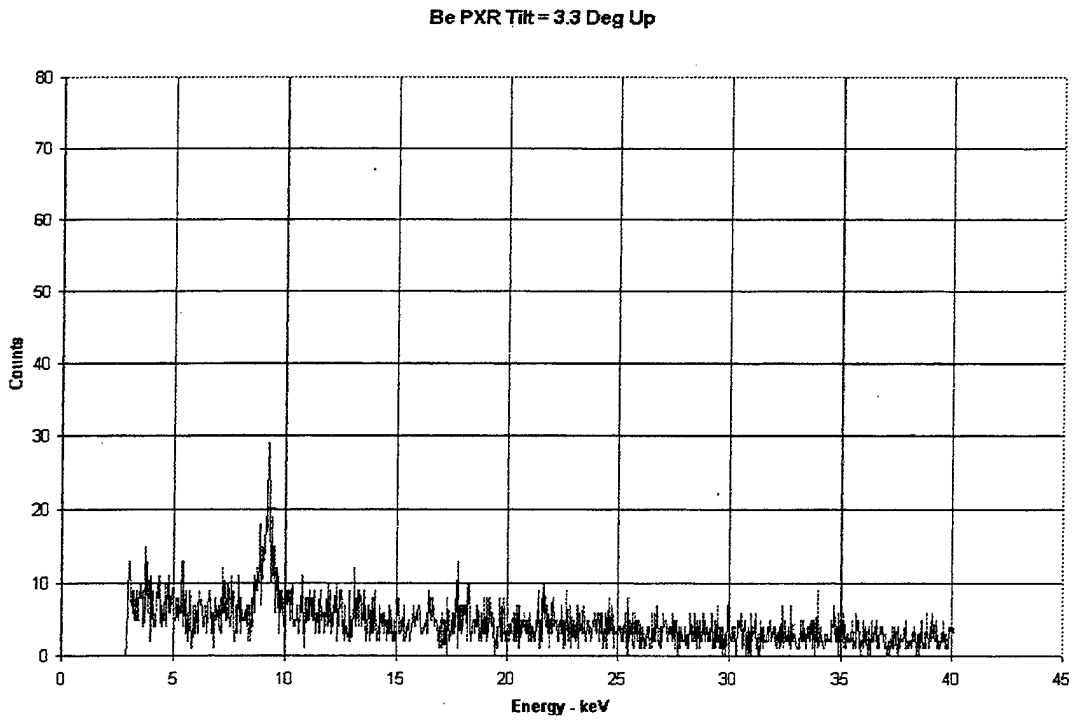

Figure 35

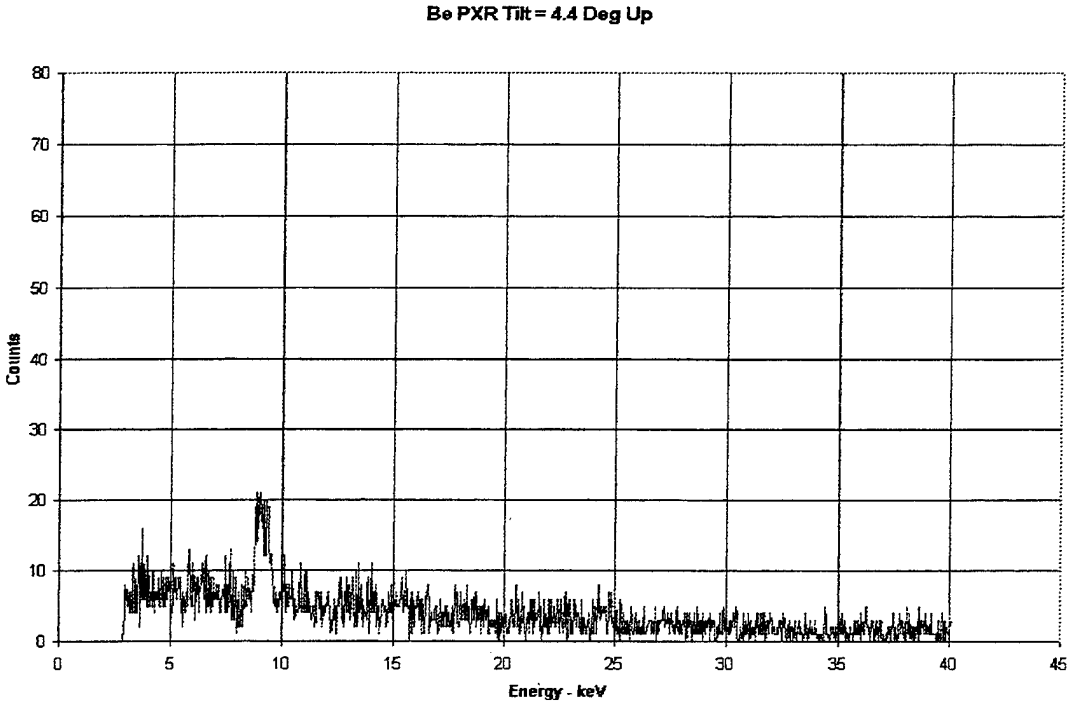

Figure 36

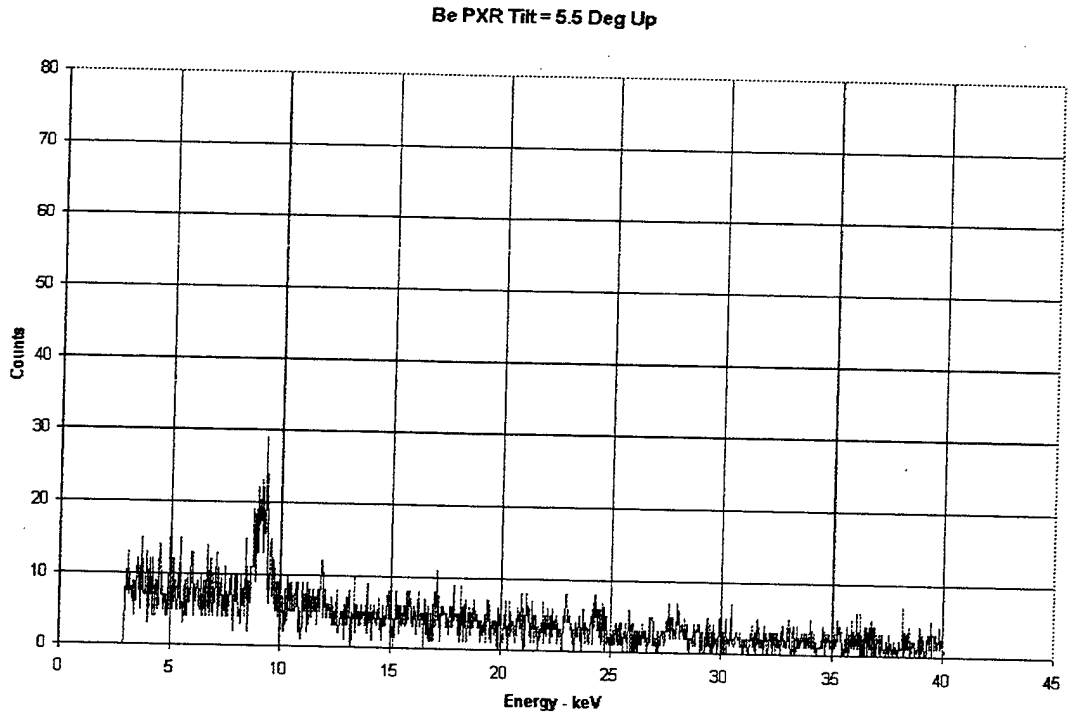

Figure 37

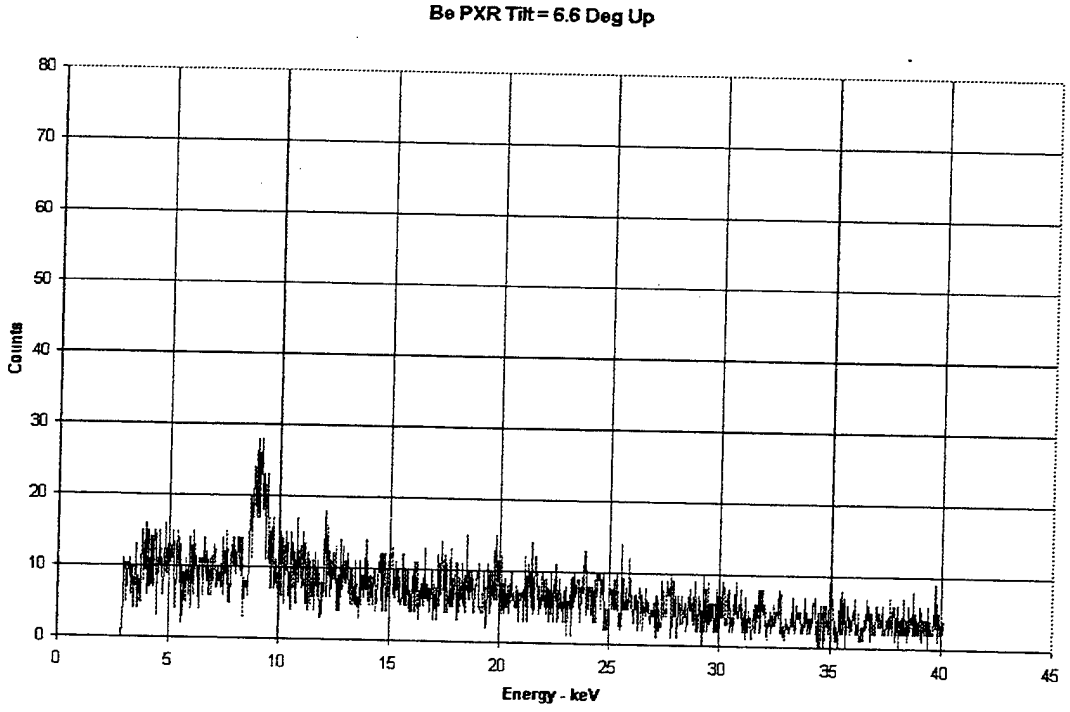

Figure 38

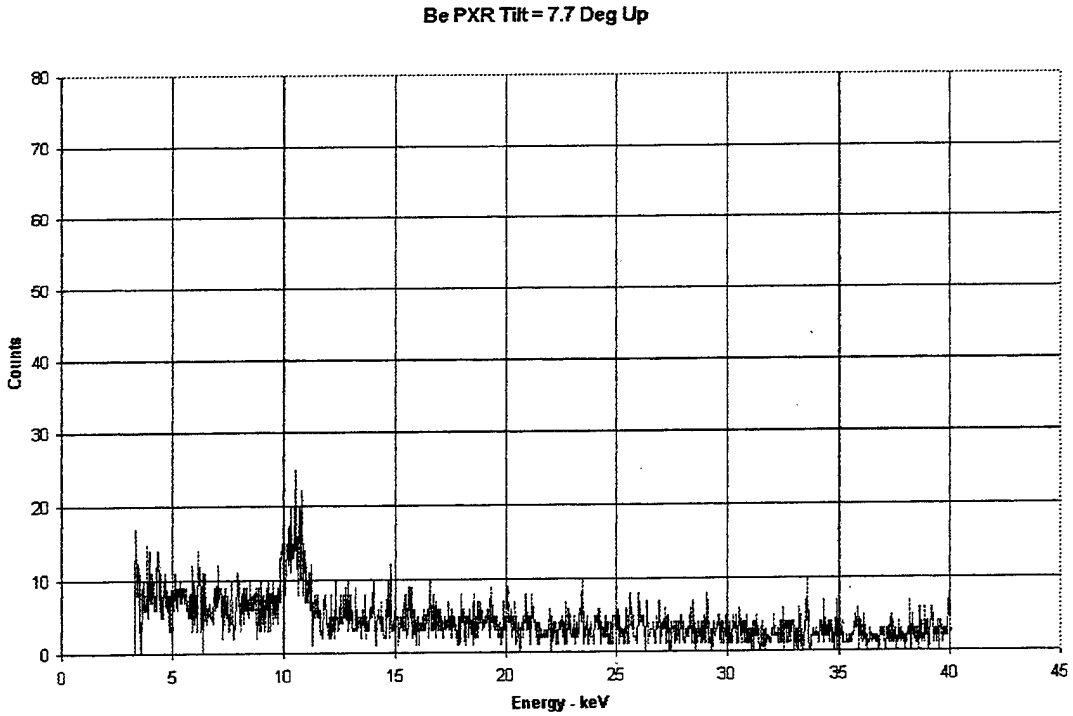

Figure 39

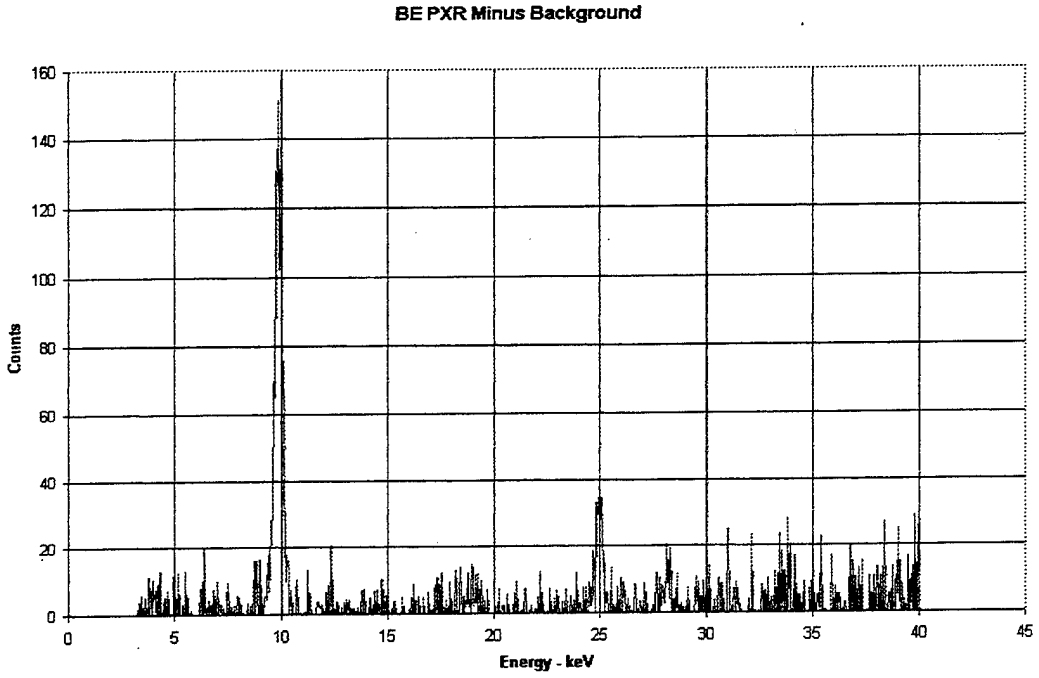

Figure 40

LIST OF REFERENCES

1. Feranchuk, I.D. and Ivashin, A.D., "Theoretical Investigation of the Parametric X-Ray Features", J Physique, v.T46, no.11, pp. 1981-1986, November 1985.

2. Cullity, B.D., Elements of X-Ray Diffration, 2nd Edition, Addison-Wesley Publishing Company, Inc., 1978.

3. DiNova, K.L., "Enhanced Higher Order Parametric X-Radiation Production", Masters Thesis, Naval Postgraduate School, Monterey, California, December 1992.

4. Fasanello, T.J., "Solid State X-Ray Detector Calibration and LINAC Beam Intensity Measurements", Masters Thesis, Naval Postgraduate School, Monterey, California, December 1992.

5. Knüpfer, W., "Feasibility Study of a Channeling Radiation Source for Applications in the X-ray Region", Nuclear Instruments and Methods in Physics Research B, 87, pp. 98-103, 1994.

6. Freudenberger, J., "Properties of Channeling and Parametric X radiation", AIP Conference Proceedings, 389, pp. 73-90, September 1996.

7. Burattini, E., Gambaccini, M., Marziani, M., Rimondi, O., Indovina, P., Pocek, M., Simonetti, G., Benassi, M., Tirelli, C., Passariello, R., Rev. Sci. Instr 63 (1992) 638.

8. Warren, B.E., X-ray Diffraction, Addison-Wesley Publishing Company, Inc., 1969.

9. Private facsimile between M. Piestrup, Adelphi Technology, X. K. Maruyama, NPS, and author.

INITIAL DISTRIBUTION LIST

1. Defense Technical Information Center.....2
   8735 John J. Kingman Rd., STE 0944
   Ft. Belvoir, Virginia, 22060-6218

2. Dudley Knox Library.....2
   Naval Postgraduate School
   411 Dyer Rd.
   Monterey, California 93943-5101

3. Professor X. K. Maruyama, Code Ph.....3
   Department of Physics
   Naval Postgraduate School
   Monterey, California 93943-5101

4. Dr. M.A. Piestrup.....1
   Adelphi Technology Inc.
   532 Emerson Street
   Palo Alto, California, 94301

5. Mr. Don Snyder, Code Ph.....1
   Department of Physics
   Naval Postgraduate School
   Monterey, California 93943-5101

6. Professor Bill Maier, Code Ph.....1
   Department of Physics
   Naval Postgraduate School
   Monterey, California 93943-5101

7. LT David J. Hauth.....1
   USS John C. Stennis (CVN-74)
   BOX 15
   FPO AP 96615-2874

8. Mr. Robert W. Hauth.....1
   7685 Feddick Rd.
   Hamburg, New York 14075